VOLUME 18, 1956/57, No. 12 pp. 349-384 Published 4th June 1957

Philips Technical Review

DEALING WITH TECHNICAL PROBLEMS
RELATING TO THE PRODUCTS, PROCESSES AND INVESTIGATIONS OF
THE PHILIPS INDUSTRIES

EDITED BY THE RESEARCH LABORATORY OF N.V. PHILIPS' GLOEILAMPENFABRIEKEN, EINDHOVEN, NETHERLANDS

A HIGH-SPEED UNISELECTOR FOR AUTOMATIC TELEPHONE EXCHANGES

by J. M. UNK *).

621.395.343

The employment of high-speed selectors is of interest in both direct and indirect systems of automatic telephony. In this article a very rapid uniselector is described. A new method o coupling it to a common driving system makes it possible to bring the selector to a stop, agains· the desired outlet, from a speed of rotation of 300 outlets per second. This speed permits the adoption of novel wiring schemes whereby wear is very considerably reduced.

Introduction

The selector is an essential element in a telephone system. Basically it is a multi-way switch, the brushes or "wipers" of which are able to travel over a number of contacts in order to establish the connection desired by the subscriber.

Some time ago in this journal a private automatic branch exchange was described which made use of the U45a [1]) high-speed uniselector recently developed by Philips Telecommunicatie Industrie. The employment of this selector has great advantages, not only in private exchanges but also in public ones, both in systems without registers (direct systems) and in those with registers (indirect systems). The selector in question will now be described and in some respects compared with other types, including the two-motion selector. The most interesting feature of the U45a, viz. its great speed, will also be given closer attention.

The construction of the two-motion selector formerly in common use, with its 10×10 contacts (outlets), is such that the wipers have only a relatively short distance to travel in order to reach any desired contact; this permits the finding time to be short and the average speed in steps per second to be relatively low. For example, in order to reach the 96th outlet from the home position, the wipers have 9 vertical and 6 horizontal steps to take, a total of 15 steps. The two-motion selector has the disadvantage, however, that the wiper mechanism is subjected to high accelerations and decelerations, resulting in severe mechanical shocks, heavy wear and high contact noise. A second disadvantage, the seriousness of which will become clear in the course of this article, is that the 100 outlets must invariably be divided into 10 groups of 10, no other groupings being possible.

The use of "one-motion" rotary selectors (uniselectors) having the same number of outlets gives much greater freedom as regards the grouping of the outlets; in a uniselector they can be distributed between various groups in any desired manner. However, in order to obtain finding times equal to or shorter than those of the two-motion selector, the speed of the uniselector wipers must be very much greater, because generally a greater distance has to be travelled. In certain circumstances it is possible to contrive that the average distance to be travelled by the wipers of the high-speed uniselectors is no greater than that for the two-motion selector. We shall come back to this point later.

*) Philips Telecommunicatie Industrie, Hilversum, Netherlands.

1) B. H. Geels, A private automatic branch exchange using high-speed uniselectors, Philips tech. Rev. **18**, 19-30, 1956/57.

In order that the U45a [2]) with its higher speed might be provided with a steady and powerful continuous drive, it was decided to run it from a central powering sytem, in other words, from a motor common to a number of selectors, each selector being driven via a coupling mechanism. The mechanism has only lightweight parts to set into motion and to arrest; in consequence, wear and selector noise are considerably reduced. Motor-driven uniselectors having a speed of 200 contacts per second have previously been developed during the last few decades. The drive of the U45a selector differs radically from that of its predecessors, however. In the U45a the speed of wiper travel has been raised to 300 contacts per second. We shall demonstrate that it is of great importance that the speed should have been raised to this particular figure, in that it permits the adoption of a new method of connecting the outlets whereby, despite the greater speed, a reduction of wear is obtained.

Positioning of a group selector in a direct system

In direct telephone systems the selectors of the various stages or steps are positioned directly, one after the other, by the impulses coming from the subscriber's dial. The functions of the various selecting steps, such as final and group selectors and line finders, are briefly explained by the diagram in *fig. 1* and the accompanying description (see also the articles cited in footnotes [1]) and [2])).

In direct systems it is necessary that the group selector should have found an idle outlet of the desired group before the following digit is dialled.

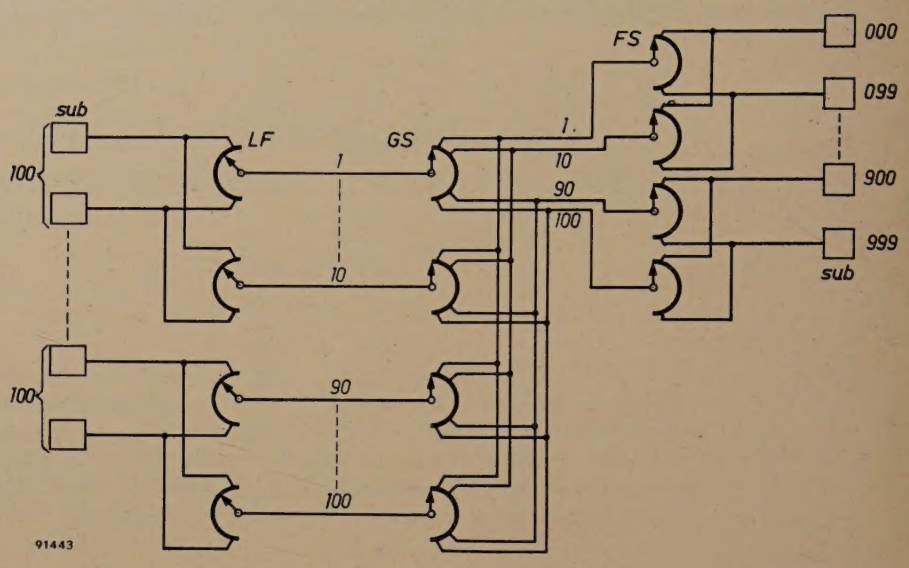

Fig. 1. Elementary scheme of connections in an automatic exchange.

Subscribers' lines (*sub*) to a telephone exchange are generally bunched in groups of 100, being connected up to contact banks of selectors having 100 outlets in order that they can be dialled. These selectors are known as final selectors (*FS*). If the exchange is to handle 100 to 1000 subscribers, group selectors (*GS*) are placed in front of the final selectors, so that an idle final selector can itself be selected as a link to the desired group of 100 subscribers. Where the subscribers number from 1000 to 10 000 a further group-selector stage is necessary in front of the group selectors just mentioned, so that a free group selector can be selected as a link to the desired group of 1000 subscribers.

In order therefore that a subscriber be able to dial, there must be a group selector available for him. Since only a small proportion of subscribers make calls at the same time, it is not desirable to connect each subscriber to the wipers of a group selector. Hence lines from subscribers are connected to a very much smaller number of group selectors via one or more reduction stages. The line finder (*LF*) is an example of a reduction stage. Subscribers' lines are connected to the contacts of the line finders, the wipers of which are connected with the wipers of the group selectors. The number of selectors that is required depends on the number and duration of calls made in the busy hour. For example, a group of 100 subscribers might be provided with 10 group selectors. In this case 10 line finders, each having 100 outlets, would be necessary. When a subscriber takes up his handset the wipers of an idle line finder start passing over the contacts in order to find the caller. For this purpose a relay connected to one of the wipers of the line finder, called the test relay, is put in circuit with the various subscribers' lines one after the other. Immediately the test relay comes into the caller's circuit it operates, thereby bringing the line finder to a halt. In order that calls already in progress between subscribers of the group should not be disturbed, this "testing" is made to take place, not through the two speech conductors, but through a third conductor. Thus not only the two speech conductors link the subscriber to the line finder; there are three conductors, frequently even four. Three or four contacts are therefore necessary for each subscriber. These contacts are placed one above the other, and hence the line finder has three or four layers of contacts and the same number of wipers, the three or four wipers meeting the three or four contacts belonging to a single subscriber. The same applies to group and final selectors, these likewise having three or more layers of contacts.

In the two-motion selector, division into groups is provided by the mechanical construction of the device (10 × 10 outlets). This is not the case in the uniselector; the grouping of the outlets of a uniselector is effected by electrical interconnection, the result of which is that the dialling of a certain

[2]) The U45a is a further development of the U45 selector also designed by Philips Telecommunicatie Industrie. On the U45, see N. Rodenburg, Een telefoonsysteem met snelle draaikiezers, De Ingenieur **63**, E83-E87, 1951 (No. 50); D. van Hemert and J. Kuin, Automatische telefonie, published by Netherlands Post Office, The Hague 1954; J. M. Unk, A new high-speed uniselector for automatic telephony, Comm. News **12**, 69-99, 1951/52.

digit causes all free outlets to the group in question to be "marked" with a suitable voltage. There is no difficulty in altering the number of outlets to be "marked" simultaneously, and hence the division of uniselector outlets into groups is very flexible. After a digit has been dialled, an idle outlet (to the final selector or the next group selector, as the case may be) has to be sought amongst the outlets thus "marked". As already stated, it must have been found before the next digit is dialled. The time available is therefore the interval between two trains of impulses, and this is dependent on the temperament of the subscriber. The shortest inter-digital pause — the minimum time between two trains of impulses — is approximately 450 msec, 350 msec of which are available for the hunting of an idle outlet. The other 100 msec will be taken up by the release action of a slow relay. If the speed of the selector is not great enough for all the outlets to be swept within 350 msec, then the positioning of the selector must start while the impulses determining the desired group are still being received (i.e. during the return movement of the subscriber's dial), in such a way that the selector arm stands in front of the outlets for that group when the impulse train comes to an end. In that case, only the contacts of the desired group will have to be hunted during the dialling pause. But this would make it necessary for the outlets of a group to be placed next to one another and for the selector arm to have a fixed home position.

If the speed of the selector is great enough for all 100 outlets to be travelled in the 350 msec available, it is no longer necessary that the selector should have a fixed home position or that the positioning should start while the train of impulses is still being received. By the same token, it is not necessary to place all the outlets of a group adjacent to each other; on the contrary, it will be of advantage to distribute them uniformly over the entire arc of the contact bank so that the outlets of various groups occur in the bank one after the other. The selector arm and the wipers will then have, on the average, only a short distance to travel before finding the first idle outlet in the desired group. This shorter distance is about one-tenth of the distance that the wipers would have to travel in the case first considered. There is no need for the selector to return to a home position once the call has finished, and consequently the selector makes only one movement per call. In this way the average finding time and the wear suffered by the selector are very considerably reduced.

The speed necessary for all 100 outlets to be passed over in approximately 350 msec is $100/0.35 \approx 300$ outlets per second.

It is desirable that line finders too should work at high speed. Otherwise there is rather a long delay before the calling subscriber hears the dialling tone. Since line finders normally have no home position, and since the wipers of a set of finders will all occupy different random positions, the delay can be cut down by having several idle finders hunting at the same time. The solution is not a satisfactory one, however, for it does not help matters much in the busy hour and the finders suffer increased wear, being set into motion more frequently than is necessary. If a line finder works at high speed it is unnecessary to have more than one engaged in hunting the call. This is so for the U45a selector, which has an *average* finding time of approximately 200 msec, inclusive of the time taken by the relays to operate.

Factors limiting the speed of the selector

The main limitation to the speed at which a given selector will work reliably is the need for it to be able to stop in time. The position at which it must come to a halt is normally determined, as stated above, by "marking" a contact with a suitable voltage. Immediately the wiper arrives at this contact, a relay (the test relay) is energized. The tripping of the relay causes the selector to be halted; this must take place so quickly that the wiper does not have time to move on from the "marked" contact. The mechanical shock occasioned by stopping must not be too great, in order that undesirable oscillation of the wipers and the jarring of vulnerable parts of the mechanism be obviated. The shock of stopping depends on the energy of rotation possessed by the selector at that instant; it is therefore of the greatest importance to keep this energy down to a minimum.

We have already said that the U45a selector is designed for a common motor drive: as and when required, the selectors are coupled to a common, continuously running motor. Frequently uniselectors are powered by their own separate motors, in which case they are referred to as motor selectors. In these circumstances the motor is responsible for the greater part of the total energy of rotation. Since this is proportional to the square of the angular velocity and to the moment of inertia of the moving parts, it is obvious that the system of common drive allows of greater speeds, for there is now no need for the motor itself to be stopped, as in the case of the motor selector. In an existing 6-arm motor selector the moment of inertia about the rotor spindle is 2885 g cm^2. If the selector works

at a speed of 200 contacts per second, the kinetic energy that has to be dissipated when it is brought to a halt is 20.5 millijoule. In a 4-arm U45a selector the moment of inertia about the rotor spindle is 732 g cm^2, and its kinetic energy at the same speed is 5.8 mJ, or about 3½ times less than the value for the motor selector. When the U45a selector works at a rate of 300 contacts per second its kinetic energy amounts to 13 mJ.

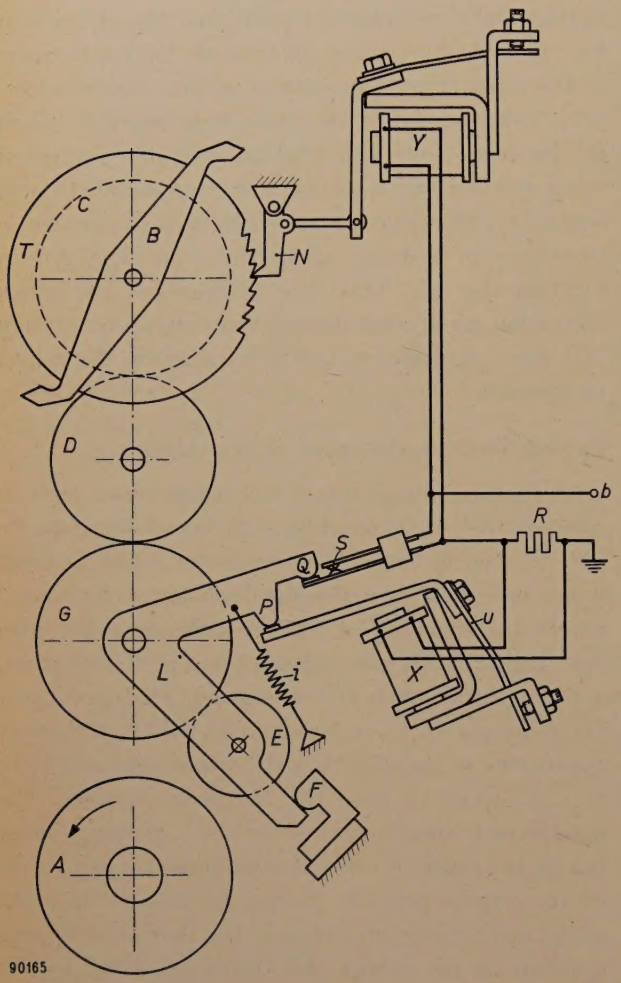

Fig. 2. Schematic diagram showing the functioning of the U45a selector. By means of arm L, which is actuated by the coupling magnet X, pinion E can be made to engage with driving wheel A. The intermediate member G consists of two gears (y and z in fig. 3) between which there is a friction coupling. C and D are further gears. B is the rotating arm bearing the wipers. T and N are ratchet wheel and pawl, the latter being actuated by electromagnet Y. Y is short-circuited via contact S. Contact at this point is broken by Q, a spur on arm L, when E is engaged with A. The arm L has a further spur P; P is raised, and the arm turned anti-clockwise, by leaf spring u acting via the armature of magnet X and overcoming the tension of spring i, until the other extremity of the arm comes up against stop F. R is a resistor.

Existing selectors with common drive are brought to a halt by withdrawing the driving force once the test relay has tripped, and subsequently applying a braking force. The time available for stopping the selector is therefore shortened by the length of time necessary for disengaging the coupling, a delay for which the inertia of the coupling is responsible. This severely limits the speed that the selector can attain. In consequence a new type of coupling was developed for the U45a selector, whereby the selector is first brought to a halt and then disengaged by magnetic means from the gear that drives it: a friction coupling between two of the gears allows them to move relative to each other in the interval elapsing between the stopping of the selector and the disengagement of the gears. Hence the inertia of the magnetically-operated coupling plays no part.

Selector mechanism

The functioning of the selector mechanism will be explained with reference to *fig. 2*. The rotor consisting of the wipers of the selector, is fixed to gear C, which meshes with gear D. G, the intermediate member, consists of two gears y and z, which are able to turn relative to each other by virtue of the friction coupling between them (see *fig. 3*). Gear z meshes with D and gear y with pinion E. Pinion E is attached to an arm L, which by turning causes the former to engage with wheel A; this last is fixed to the continuously rotating shaft of the common drive motor.

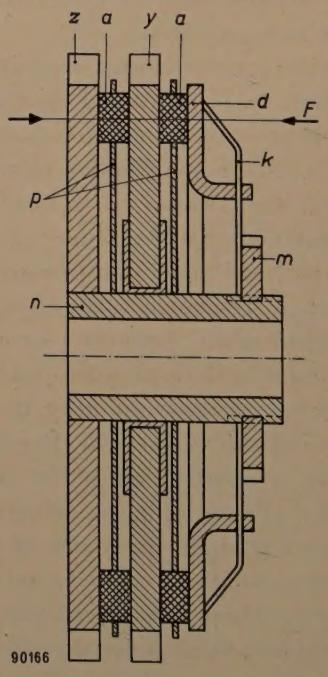

Fig. 3. Intermediate member (G in fig. 2), consisting of gears y and z and friction blocks a, which are kept in place by plates p. F, the force with which the gears and friction blocks are pressed together, is exerted by spring k via tension plate d, and can be regulated by means of nut m. Gear z is fixed with respect to sleeve n.

Fixed to the spindle of gear C is a ratchet wheel T; a pawl N, actuated by electromagnet Y, engages in the ratchet wheel. When the selector is at rest, the spring u of the armature of the coupling magnet X presses arm L against stop F. Electromagnet Y is short-circuited via contact S. When voltage is applied to terminal b of the selector, all that happens in the first place is that coupling magnet X pulls its armature over. Arm L is now caused by tension spring i to turn clockwise, thus coupling pinion E with wheel A. Spur Q on arm L breaks contact S only after the teeth of E and A are partially engaged, and only then is electromagnet Y energized and the pawl withdrawn from ratchet wheel T. Resistor R prevents sparking at contact S when the latter breaks, and also serves to reduce the reactance of the current path, thus causing electromagnet Y to release its armature more quickly when the flow of current is stopped. In consequence of the fact that E and A are already partially engaged, and that therefore gear y in intermediate member G is already turning, there is slipping of the friction coupling in G and a torque is exerted on gear z, which meshes with D. Thus the wipers start to turn immediately the pawl retracts. This sequence of events means that the friction coupling absorbs the shock resulting from the meeting of the wheel A and the pinion E, and hence there is no question of the wipers undergoing excessive acceleration.

The torque transferred by the friction coupling (see fig. 3) is proportional to the coefficient of friction between the blocks and the steel gears. For the frictional material employed (leather blocks impregnated with a silicon oil), the static coefficient of friction is less than the kinetic, and this latter increases with the amount of slip. The torque is therefore strongest at the moment the pawl retracts, for that is the time when the greatest amount of slip occurs. In consequence, the selector is brought up to its normal speed in the shortest possible time. While it is thus being speeded up, the amount of slip between gears y and z decreases, with the result that the torque decreases and the acceleration of the wipers proceeds very evenly. Because the coefficient of friction for the material employed decreases with increasing temperature, it will never heat up to excessive temperatures and, at the normal rate of rotation, the friction coupling will allow continuous slipping to take place without exhibiting perceptible wear or any tendency to jam.

When the selector has to be stopped, the flow of current through stopping magnet Y and coupling magnet X is broken by the test relay. Release by the stopping magnet of its armature causes the pawl to arrest the ratchet wheel (and hence the wipers); spring u causes arm L bearing pinion E to turn anticlockwise, thus disengaging E from A. In the interval elapsing between the stopping of the wipers and the disengagement of the selector there is slipping of the friction coupling. The torque that continues to be exerted on C and hence on ratchet wheel T serves to counteract bounce. Since the torque increases with the amount of slip, the braking torque on the rotor during its small backward movement following bounce is on the average greater than the driving torque exerted in forward movement. The absorption of the kinetic energy of the rotor by friction between wipers and contacts and the elastic deformation occasioned by collision between pawl and ratchet also contribute to the reduction of bounce. At each collision about half of the energy is dissipated. All these effects result in the rotor coming practically to a halt after the second bounce.

The movement of the wipers in relation to the contacts when the selector stops is shown in *fig. 4*. It is quite clear from the graph that the wipers do not fly past the contacts when the ratchet wheel bounces back from the pawl; indeed, there is a considerable margin of safety.

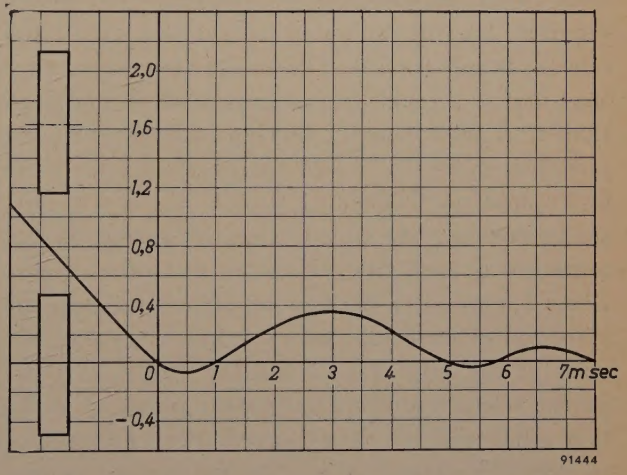

Fig. 4. Displacement/time diagram showing the stopping of the selector (which has a speed of rotation of 300 contacts per second). The width and position of two successive contacts are indicated on the left.

The U45a selector as described here has a separate ratchet wheel for the stopping mechanism. In other designs use is made of the final gearwheel on the wiper spindle. In this case, however, the tooth flank that comes up against the pawl is not perpendicular to the line OO' (see *fig. 5a*). The consequence is that there is a fairly strong force tending to push the pawl out of the teeth when the selector

is halted, and a force F_a has to be exerted on the pawl in order to prevent this happening. Where an independent ratchet wheel is employed its teeth can be cut in such a way that the flank is perpendicular to OO' (see fig. 5*b*), so that there is not the slightest tendency for the pawl to be thrown out

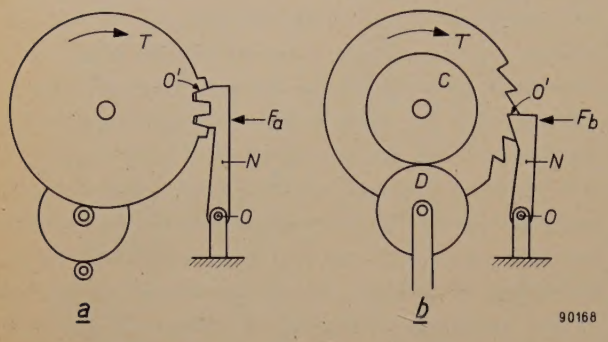

Fig. 5. *a*) Gearwheel T and pawl N for stopping the selector. The flank of the tooth at O' is not perpendicular to a line drawn from O to O'.
b) Ratchet wheel T and pawl N for stopping the selector. Here the flank of the tooth at O' is perpendicular to OO'.

of the ratchet. A weak force (F_b) exerted by the armature of the stopping magnet on the pawl suffices to prevent its ejection, and this makes it possible for the armature of the magnet to be of quite light construction. Accordingly, the power required for the stopping magnet in the U45a selector is only 6 watts. This has the advantage that the current through the magnet is weak, so weak that if a fault should develop and the winding remain in circuit, it would not overheat and therefore would not burn out. Despite the weak energizing current, the pressure of the spring on the armature is such that the pawl halts the ratchet wheel 1 msec after the flow of current through the stopping magnet has been broken, reaching the apex of the ratchet trough after 1.2 msec. Tests on the selector in a special circuit (in place of the test relay circuit) have proved it to be possible to stop the selector at any desired contact from a speed of 700 contacts per second.

Apart from the shape of the teeth, the diameter of the ratchet wheel is of great importance. For a given total kinetic energy, the shock (change of momentum) when the ratchet wheel collides with the pawl decreases proportionally as the diameter of the wheel increases. On the other hand, the moment of inertia of the wheel increases as the fourth power of its diameter. For a given speed of rotation, therefore, the kinetic energy of the ratchet wheel, and hence the total kinetic energy, increases rapidly with the diameter of the wheel. There is a certain diameter of the wheel for which the shock of collision is at a minimum. For a U45a selector with 102 outlets and 6 wipers it is round about 70 mm, and this is the diameter that has been chosen for the ratchet wheel. Life tests have demonstrated that ratchet and pawl suffer no marked wear after having acted 10^7 times; this is equivalent to 10^7 calls, or a call every five minutes for a century.

In general, the total kinetic energy to be dissipated per call gives a measure for wear on the selector and for contact noise. The energy to be dissipated per call in a U45a selector working at a speed of 300 contacts per second is approximately 13 mJ. The equivalent figure for the earlier-mentioned motor selector working at a speed of 200 contacts per second (this involving two halts per call) is approximately 41 mJ in all. In the two-motion selector working at a speed of 10 steps per second during vertical movement and 30 steps per second during rotary movement, the total energy to be dissipated per call amounts to approximately 400 mJ.

Constructional details of the selector

The ratchet wheel in the standard version of the U45a selector is provided with 102 teeth, each tooth corresponding to an outlet. The selector therefore has 102 outlets. The contacts of these outlets (there may be 4 or 6 contacts for each outlet, arranged in 4 or 6 layers — see account under fig. 1) together form the contact bank. In order to make it possible to extract the wiper mechanism, these contacts are not distributed over the full circumference of a circle; instead, the 102 contacts of each

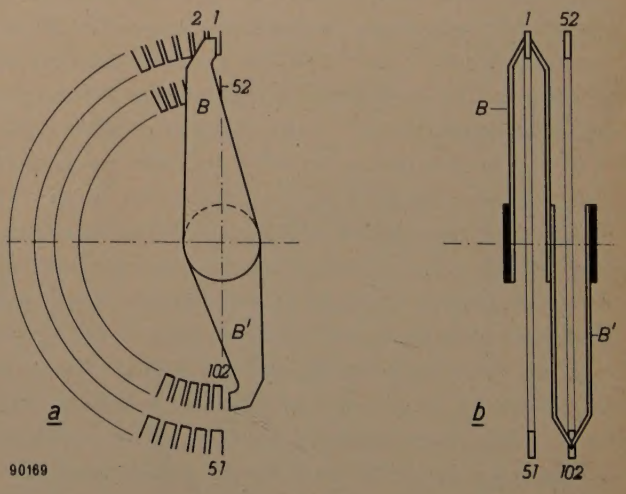

Fig. 6. Diagram to show distribution of 102 contacts over two arc-shaped rows. In (*a*) for the sake of clarity, the arc containing contacts 52-102 is drawn with a smaller radius than the arc containing contacts 1-51 and wiper B' is drawn smaller than wiper B. The true proportions are given in the side-view (*b*).

layer are divided into two 180° arcs of 51 contacts each. The two arcs are fixed side by side. The selector has two wipers for each layer; the two wipers are diametrically opposed and each travels over an arc in its turn. The arrangement is shown in *fig. 6*. For the sake of clarity, fig. 6*a* has been drawn in such a way that the radius of one arc of contacts, and the wiper for that arc, appear longer than the radius and wiper of the other arc, although in reality they are identical and situated adjacent to each other. Wiper *B* travels over contacts 1-51; as soon as it leaves contact 51, wiper *B'* arrives at contact 52 and passes successively over the contacts up to 102.

If desired, the number of outlets on the selector can be reduced to 51. There is then only one arc of 51 contacts per layer, these 51 contacts being distributed over 180°. In this case, the single arc is travelled by a single wiper with two ends, so that the wiper reaches contact 1 immediately after its other end leaves contact 51 (see *fig. 7*). The selectors can be made with any desired number of layers up to 16. Since it is not economic to keep a variety of kinds in stock, two standard versions are produced, one with 4 and one with 8 layers.

A selector with 4 wipers and 102 outlets appears in *fig. 8*; *fig. 9* shows the wipers complete with the driving mechanism. This unit can be extracted

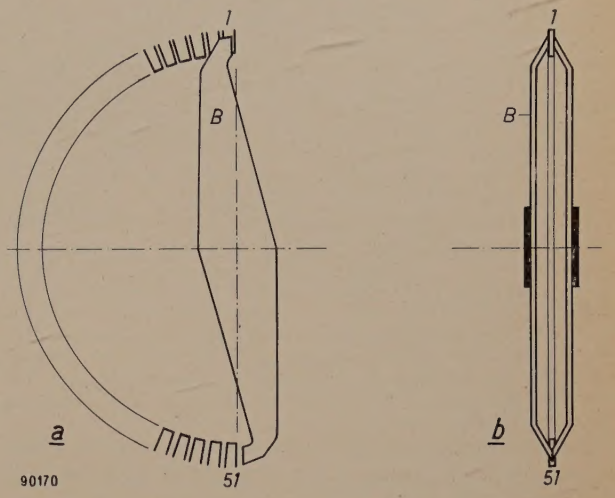

Fig. 7. *a*) Simplified diagram of selector having 51 contacts and double wiper arm *B*. *b*) Side-view of the same.

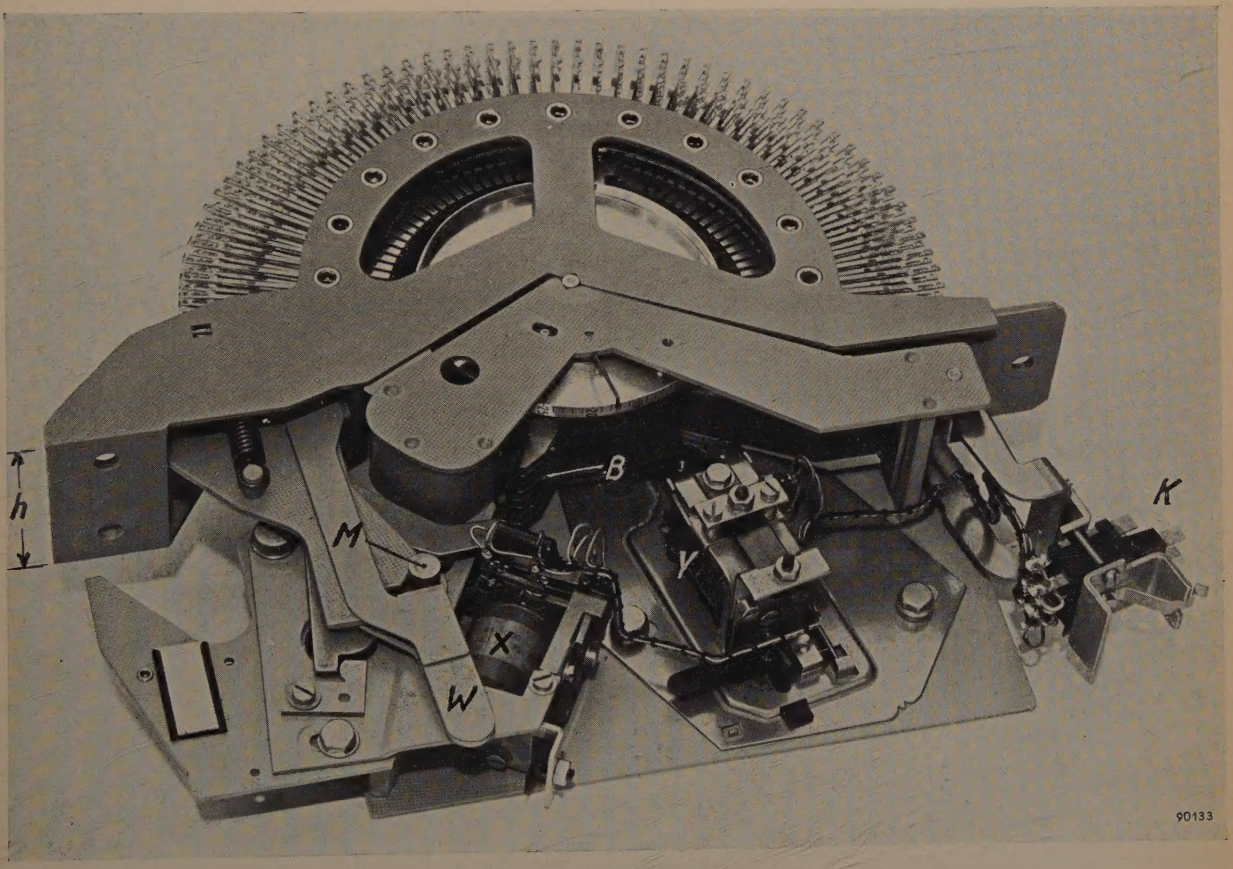

Fig. 8. U45a, a high-speed uniselector with four wipers and 102 outlets. *X* and *Y* are the coupling and stopping magnets respectively. *W* is a lever which, by means of a pin *M*, retains the wiper mechanism in the contact bank. *K*: knife contacts for electrical connections to magnets *X* and *Y* and wipers *B*. The overall breadth of the selector is $h = 49$ mm.

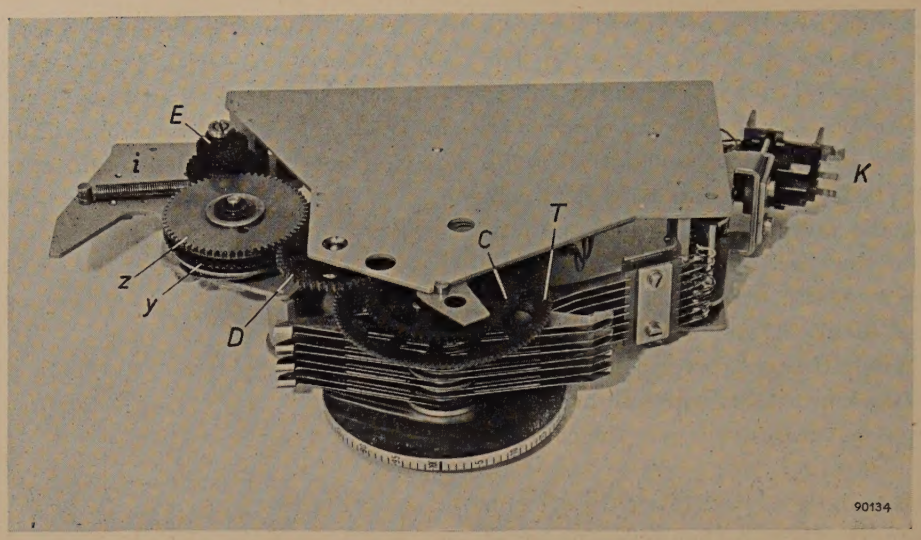

Fig. 9. Wiper mechanism with four wipers. y and z are gears of the intermediate member, E is the coupling pinion, C and D are gears, T is the ratchet wheel, i the tension spring (see fig. 2) and K the knife contacts.

from the contact bank in a simple fashion, even while in operation. First the knife contacts K are released (see fig. 8) by turning the arm on which they are mounted. Lever W is then moved to the left, thereby freeing the pin M and making it possible to take the whole wiper unit out of the contact bank. Lever W is provided with a spring whereby a force is exerted on pin M, and whereby the sta-

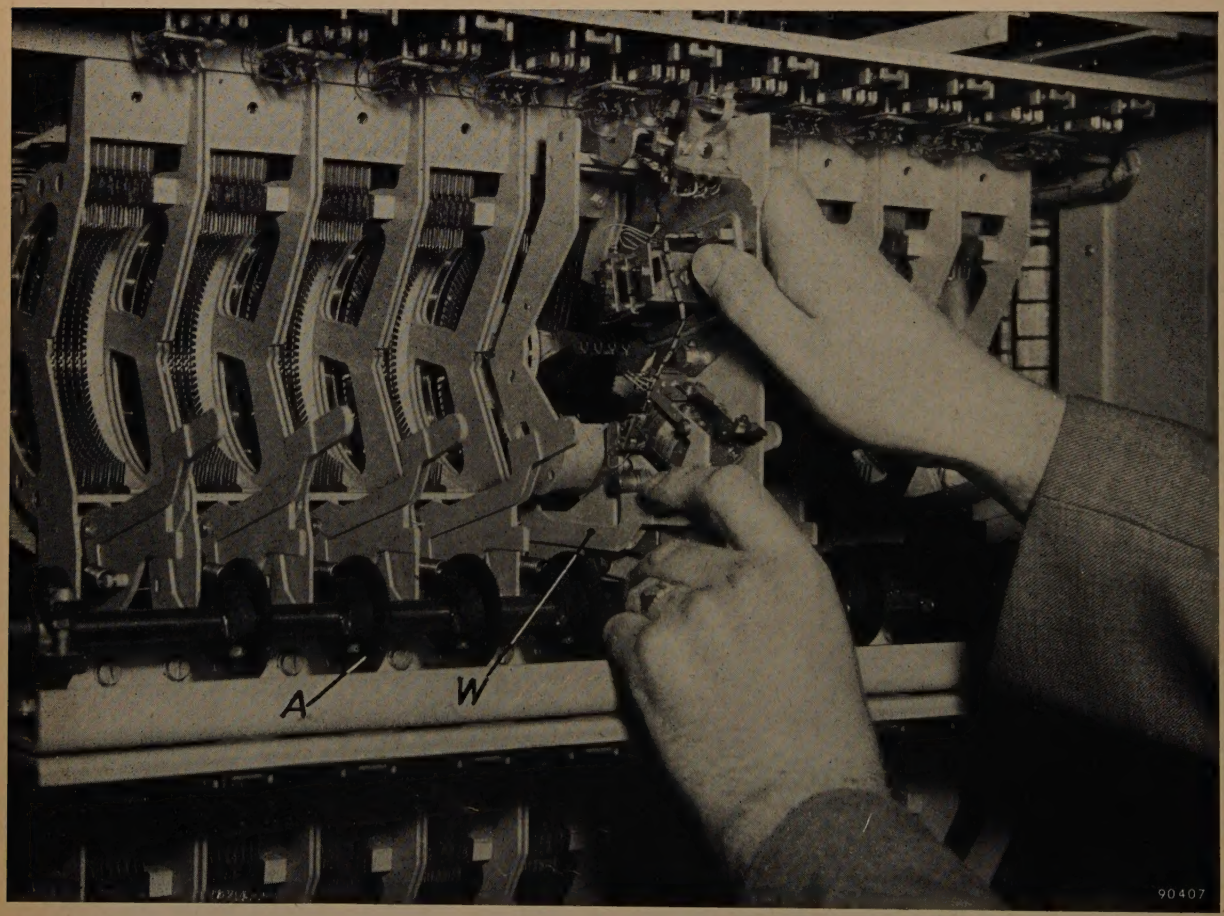

Fig. 10. Inserting a four-wiper selector in a rack. A is the continuously rotating shaft of the common drive. W is the lever shown in fig. 8.

tionary spindle on which the wipers and ratchet wheel rotate is pressed into two V-shaped recesses in the end-plates of the contact bank, good centering thus being ensured. Provision has been made for easy adjustment of the positions of the coupling and stopping magnets on the mounting-plate of the wiper unit. This is necessary in order that, when the wiper unit is inserted in a contact bank for the first time, the coupling magnet may be correctly placed in relation to the driving shaft and the stopping magnet may be so positioned that the wipers stop in the right place on the contacts.

The selectors are mounted in the rack side by side in groups, the contact banks being arranged vertically (*fig. 10*). The horizontal driving shaft for each group is itself driven by a chain common to the whole rack. Chain transmission has the advantage of enabling the racks to be fairly light in construction, for it will not be affected by vibrations in the building or by slight departures from exactness in the mounting of the horizontal driving shafts. The chains are driven off a horizontal shaft along the foot of each row of racks. Should any of the chains be too heavily loaded, it is automatically disengaged from the main driving shaft. It is possible to operate these safety couplings by hand.

Summary. The importance of high speed in automatic telephone selectors is discussed with reference to several examples of such devices. It is demonstrated that, where one-motion selectors (uniselectors) are employed, it is advantageous to make them work at a speed such that at least 300 outlets can be swept per second. There is then no need for the selector to have a home position and, furthermore, it is possible for outlets of groups to be distributed uniformly over the whole of the contact bank. This offers the great advantage that only one movement is made per call, the average distance travelled per call being one-tenth of that which would have to be travelled if there were a home position. In this way the average finding time and the wear suffered by the selector are greatly reduced. In the U45a rotary selector developed by Philips Telecommunicatie Industrie, the speed mentioned above is attained by employing a common driving mechanism with gear transmission and a new kind of coupling, whereby the selector is first brought to a halt and then disengaged. A friction coupling between the gears allows them to move relative to each other in the time intervening between stopping and the disengagement of the drive.

THE EVOLUTION OF THE PERMANENT MAGNET: A BRIEF REVIEW

621.318.2

In evaluating a material for making permanent magnets it is the magnetic properties that are of primary interest. Many other properties play a secondary part, such as workability, resistance to oxidation, the stability of the magnetic properties and, finally, the availability of raw materials and the price of the magnet.

The quality of a magnetic material as regards its magnetic properties can be characterized fairly well by the maximum value, as occurring in the demagnetization curve, of the product of induction B and the corresponding field strength H. The product $B \times H$ defines the magnetic energy obtainable per unit volume of the magnetic material when placed in a magnetic circuit to give a field in an air gap. The greater $(BH)_{max}$, the smaller are the dimensions with which the magnet can be made in order that it should possess a specified total magnetic energy (i.e. create a specified magnetic energy in an air gap). It is then, of course, necessary to design the magnet and the magnetic circuit in such a way that the operating point on the demagnetization curve is precisely that point at which the BH product has its maximum [1] $(BH)_{max}$.

The photograph will serve to illustrate the evolution of the permanent magnet from the point of view of the $(BH)_{max}$ value. It shows a series of magnets made of different materials, each magnet being of such a volume that they would all give the same total magnetic energy in a (hypothetical) air gap. Each magnet has in fact a cross-section and a length such that, when used at their $(BH)_{max}$ point, all magnets supply the same flux ($B \times$ area of cross-section) and the same magnetomotive force ($H \times$ length). A well-designed loudspeaker assembly served as basis for the choice of these values of flux and magnetomotive force. Needless to say, the new magnets designed to give those values would not fit into the magnetic circuit of the original assembly and, were the original circuit adapted to

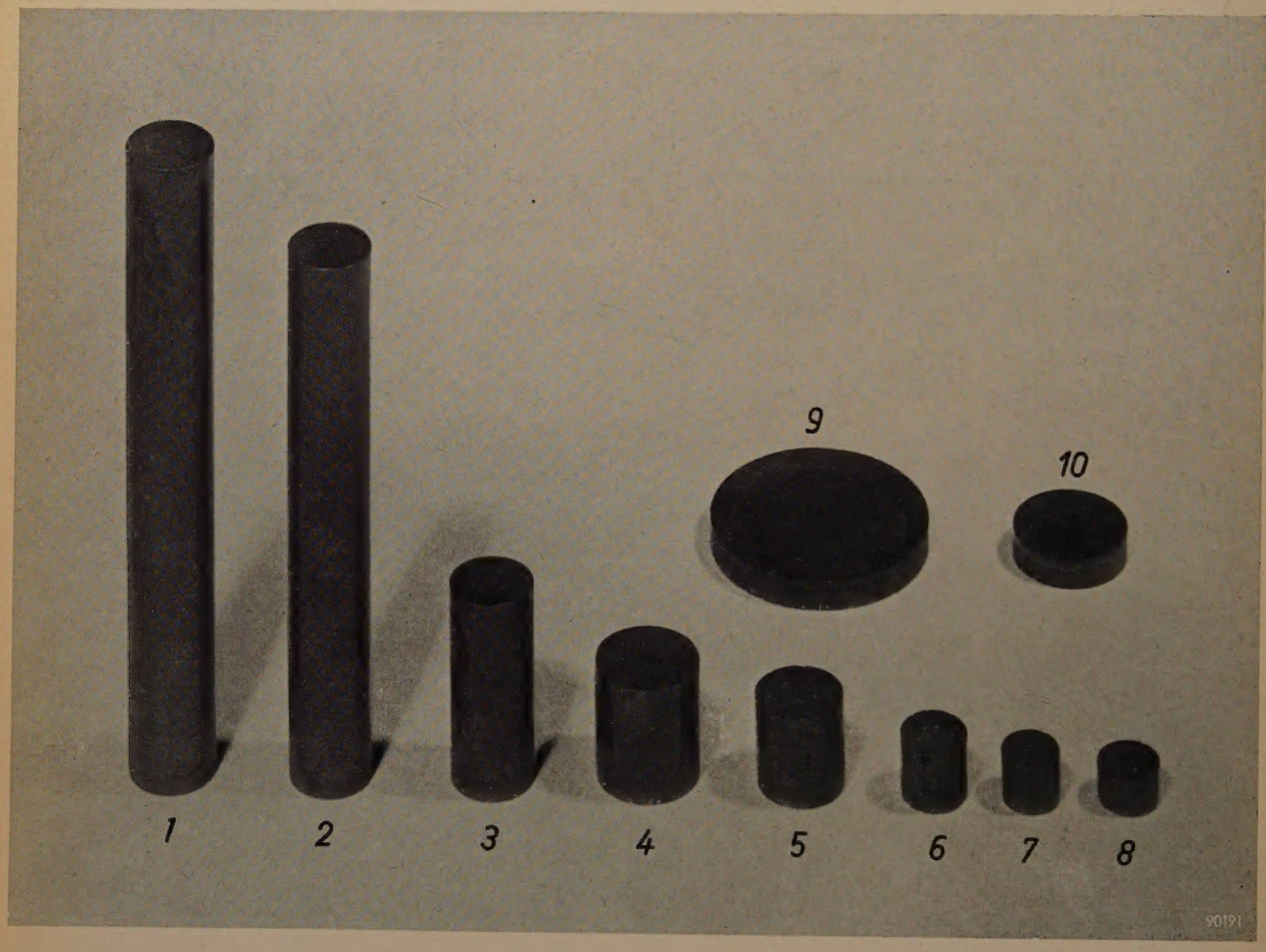

[1]) For the design of permanent magnet circuits, see for example A. Th. van Urk, Philips tech. Rev. 5, 29-35, 1940.

the new magnets, the complication of a different stray field would arise (see the article cited in footnote [1]). If we leave this correction aside, however, the photograph gives a striking picture of the progress that the development of new materials has rendered possible, and also of the effect of their development on the proportions of magnets. Some details of the materials used for the magnets in the photograph will now be given (see also the table below).

On the extreme left is a magnet made of the oldest kind of magnetic steel, namely carbon steel having a $(BH)_{max}$ of 0.26×10^6 gauss.oersted [2]). Next to it is a magnet of tungsten steel (almost identical with chrome steel, both being developed before the first world war) having a $(BH)_{max}$ of 0.36×10^6. In 1917 Honda steel appeared; it contained cobalt and had a much higher $(BH)_{max}$ value, viz. 0.9×10^6 for the magnet shown, which is of steel with 35% cobalt. This steel differed to such an extent from the types then known, both in the attainable magnet dimensions and in price (cobalt is about one hundred times dearer than iron), that years passed before it came into general use; the then youthful radio industry, in which stronger yet smaller and lighter magnets were in demand for loudspeakers, was largely responsible for its introduction. The fourth magnet in the photograph is of Mishima alloy, a magnetic alloy based on nickel-aluminium-iron, which was developed in Japan in 1933 and which has the somewhat higher $(BH)_{max}$ of 1.05×10^6. The price of such a magnet is about a third of that of an equivalent cobalt-steel magnet. Experiments on the addition of other metals to the alloy, mainly cobalt, titanium and copper, and on strictly controlled heat treatment, were successful in further improving the properties of Mishima alloy. In this way "Ticonal" II was developed, this having a $(BH)_{max}$ of 1.8×10^6; it was taken into production about 1936.

In 1938 an important step in the evolution of magnet steels was made in the Philips laboratories, when Jonas introduced heat treatment in a magnetic field [3]) for certain well-defined groups of

Table. Further data on the materials from which the permanent magnets shown in the photograph were prepared. Magnet 7a does not appear in the photo, but its material is discussed in the text.

No. in photo	Year	Designation	Magnetic properties					Dimensions of magnets		
					At optimum working point					
			B_{rem} (gauss)	$H_{coërc}$ (oersted)	B (gauss)	H (oersted)	$(BH)_{max}$ (10^6 gauss × oersted)	Diameter (mm)	Length (mm)	Weight (gm)
1	1880	Carbon steel	10000	50	5400	48	0.26	19	136	294
2	1900	Tungsten steel	11000	70	6000	56	0.34	18	115	225
3	1917	Cobalt steel 35% (Honda)	9200	240	6000	150	0.90	18	43	83
4	1938	Ni-Al alloy (Mishima)	6100	480	4050	260	1.05	22	25	69
5	1936	"Ticonal" II	6300	780	5300	340	1.80	19	19	37
6	1937	"Ticonal" G (anisotropic)	13000	580	10000	500	5	14	13	14.5
7	1949	"Ticonal" GG *) (orient.cryst.struct.)	14500	720	13000	640	8.3	12	10	8.5
7a	1953	"Ticonal" X (great coercivity)	9000	1250	5000	900	4.5	19.5	7.2	16
8	1956	"Ticonal" XX *)	11800	1315	9200	1200	11.0	14.7	6	7
9	1952	Ferroxdure I	2000	1800	1000	900	0.9	44	7.2	53
10	1954	Ferroxdure II	3750	1300	2640	1100	2.9	27	6	17.2

*) Material prepared on laboratory scale.

[2]) The values of the $(BH)_{max}$ product are given in gauss oersted in accordance with established practice, rather than in rationalized Giorgi units commonly used in this Review. In the rest of the article units will be omitted when $(BH)_{max}$ values are quoted.

[3]) Netherlands Patent No. 53734; B. Jonas and H. J. Meerkamp van Embden, Philips tech. Rev. **6**, 8-11, 1941. A short time previously Oliver and Shedden (Nature **142**, 209, 1938) had carried out similar tests on magnetic alloys already in use, producing a very slight improvement in their properties. Owing to an incorrect interpretation of the phenomenon, these investigators did not at the time continue their observations.

alloys containing nickel, cobalt, aluminium, copper and iron (and in certain cases other elements such as titanium). In this way the $(BH)_{max}$ value was raised to over 5×10^6 (in "Ticonal" G, the sixth magnet from the left). So important was this step that, even today, about a half of the world production of magnets is carried out according to the process.

In the years following 1933 much work was devoted to the problems of magnetism all over the world. Understanding of magnetic phenomena was deepened by investigators such as Néel, Snoek, Kersten and many others, and various new materials were discovered, such as the iron-cobalt-molybdenum alloys of Sykes and Köster, the cunico and cunife of Dannöhl et al., the cobalt-platinum alloys of Jellinghaus, the "Vicalloy" of Nesbitt et al., the powdered magnetic materials of Néel and the "Bismanol" (bismuth-manganese alloy) of Guillaud and the Naval Ordnance Laboratory in Washington. Considerations of cost price or practical difficulties, or both, prevented these materials being applied except in rare cases, however.

It was not until 1949 that $(BH)_{max}$ was further stepped up. The normal "Ticonal" alloy was so' dified from the melt in a special manner so t'at the crystals of the material obtained had a certain orientation. By subjecting magnets of this kind to the heat treatment previously devised [4]), very high values of $(BH)_{max}$, rising to 8.4×10^6, were attained in the laboratory. It was found possible to produce these materials on a larger scale with $(BH)_{max}$ values of 6.5 to 7.5×10^6.

In the meantime efforts have continued to raise $(BH)_{max}$ still higher. In recent years the record has been held by the American General Electric Co. with a cobalt-platinum alloy. The alloy had been described by Jellinghaus much earlier; however, in 1955, by subjecting it to a heat treatment which ordered the crystal lattice, Martin and Geisler [5]) raised its $(BH)_{max}$ value to 9×10^6. Its price naturally prohibits the extensive employment of this material.

The record has now been broken again in the Philips laboratories at Eindhoven. Earlier, a method had been discovered of increasing the coercive force of "Ticonal" alloys. The method consists of the addition of titanium and the raising of the cobalt content [6]), combined with a special kind of heat treatment [7]). It is possible thus to prepare materials ("Ticonal" X) with a coercivity H_{coerc} of 1300 Oe and a $(BH)_{max}$ of 4.5 to 5×10^6. In the course of attempts to improve this material still further by solidifying it in the desired orientation, Luteijn and De Vos succeeded a short time ago in obtaining, in the laboratory, magnets having crystal orientation with a $(BH)_{max}$ of 11×10^6 [8]); for this purpose they worked with very pure constituents, fusing them in an inert atmosphere. In the row of magnets shown in our photograph, the one on the extreme right, the smallest of all, is made of this material.

In addition, the photograph shows two permanent magnets made of ferroxdure, a ceramic (non-metallic) material; these two have the same flux and same magnetomotive force, and hence the same magnetic energy, as the other magnets appearing in the picture. Although the development of ferroxdure [9]) was governed by quite other considerations than the attainment of extremely high $(BH)_{max}$ values, it is instructive to include these two magnets in the series; the relatively low remanence but extraordinarily high coercive force of ferroxdure result in the rod form of the magnet we started with becoming a disc. The $(BH)_{max}$ of ferroxdure I lies in the vicinity of 0.9×10^6; in the meantime this value has been raised to above 3×10^6 (maximum 3.8×10^6) for ferroxdure II, this having been achieved by aligning the particles of the basic material in a magnetic field prior to sintering. It may be remarked that both the great coercive force of this material, and its non-metallic character, has resulted in a wide range of special applications.

[4]) Netherlands Patent No. 71925.
[5]) D. L. Martin and A. H. Geisler, J. appl. Phys. **24**, 498, 1953.
[6]) Netherlands Patent Nos. 70092 and 70424.
[7]) Netherlands Patent applied for.
[8]) A. I. Luteijn and K. J. de Vos, Philips Res. Rep. **11**, 489-490, 1956.
[9]) J. J. Went, G. W. Rathenau, E. W. Gorter and G. W. van Oosterhout, Philips tech. Rev. **13**, 194-208, 1951/52; A. L. Stuijts, G. W. Rathenau and G. H. Weber, Philips tech. Rev. **16**, 141-147, 1954/55.

H. J. MEERKAMP van EMBDEN.

A LOW-NOISE KLYSTRON WITH HIGH POWER OUTPUT

by R. A. LA PLANTE *) and G. A. ESPERSEN *).

621.373.423

Among the tubes used for generating a continuous high power at high frequencies the velocity-modulation valve or klystron occupies an important place. In this article the authors describe an investigation on the noise of these tubes. The principle cause was shown to be situated in the tuning mechanism. A non-tunable tube, constructed as a result of these experiments, shows a very low noise-level and has also some other favourable properties.

Velocity-modulation valves or klystrons have already been dealt with in two previous articles in this Review [1]). For a description of the working principles we refer therefore to these papers. In the second of them construction details were given of some tubes developed for wavelengths between 15 and 3 cm (frequencies between 2000 and 10 000 Mc/s). In this article we will describe some recent investigations on the subject of klystrons, more expecially with regard to the causes of noise in these tubes. We will also describe the construction of a klystron that has been developed as a corollary to these investigations.

Construction of a 3 cm klystron

Fig. 1 shows a simplified cross-section of a 3 cm klystron developed in Eindhoven some years ago. The construction is basically the same as that of the tubes described in the second article mentioned under [1]), the principle difference being that the output cavity resonator is not coupled to the waveguide by a loop but by a gap in the resonator wall, the gap being connected to a waveguide flange via a tapered waveguide. The vacuum seal is obtained with a mica window of thickness 50 microns. The tube has an L cathode [2]) which, even at the high emission density required, has a useful life of more than 1000 hours. This tube delivers a power output of 200 W at an anode voltage of 8800 V, and has an efficiency of 13%.

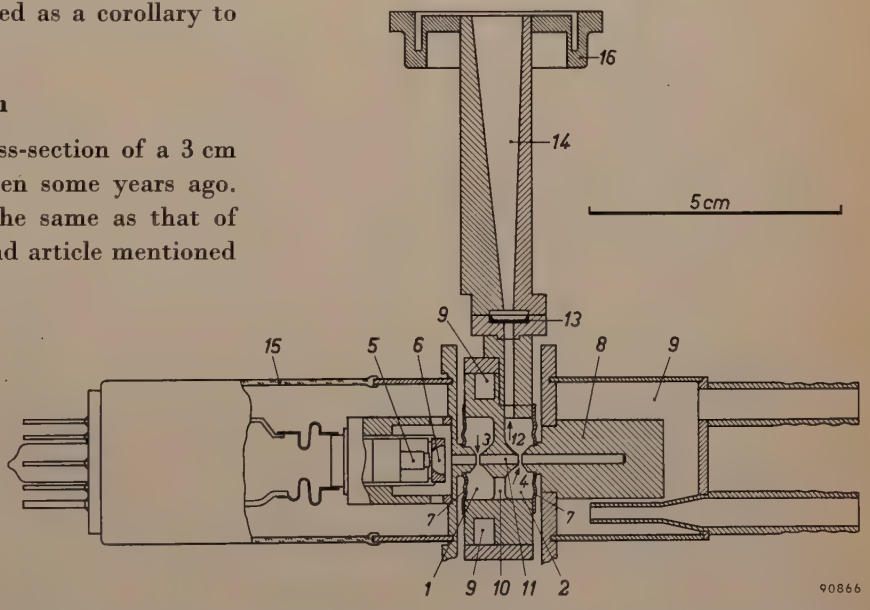

Fig. 1. Cross-section of a tunable klystron for a wavelength of 3 cm. Various details, including the tuning mechanism, have been omitted. *1* modulating cavity, *2* output cavity, *3* modulating gap, *4* inductor gap, *5* cathode, *6* focusing electrode ("grid"), *7* diaphragms, *8* collector, *9* cooling jacket, *10* feedback hole, *11* drift tube, *12* coupling gap, *13* mica window, *14* tapered waveguide, *15* glass envelope, *16* waveguide flange.

Noise of a klystron

As with all oscillators, the currents and voltages generated in a klystron are not purely sinusoidal but are subject to variations both in amplitude and phase. This also applies, therefore, to the electromagnetic field in the waveguide coupled to the tube. In many cases this deviation from a purely sinusoidal waveform manifests itself as noise, which restricts the usefulness of the tube. For instance, noise in klystrons used in beam transmitters reduces the range of the transmitter and may also limit the number of non-interfering channels permissible in a given frequency band [3]).

In the ideal case of a completely noise-free signal the field at every point in the waveguide would vary as a function of time according to $A \cos \omega_0 t$.

*) Philips Laboratories, Irvington-on-Hudson, N.Y., U.S.A.

[1]) F. M. Penning, Velocity-modulation valves, Philips tech. Rev. **8**, 214-224, 1946, and B. B. van Iperen, Velocity-modulation valves for 100 to 1000 watts continuous output, Philips tech. Rev. **13**, 209-222, 1951/52.

[2]) H. J. Lemmens, M. J. Jansen and R. Loosjes, A new thermionic cathode for heavy loads, Philips tech. Rev. **11**, 341-350, 1949/50.

[3]) See C. Ducot, Beam transmitters with double frequency modulation, Philips tech. Rev. **17**, 317-327, 1955/56.

For variations in amplitude A and in phase $\omega_0 t$ the formula for the field may be written as:

$$A\{1 + a(t)\} \cos\{\omega_0 t + p(t)\},$$

where $a(t)$ and $p(t)$ are random time functions.

It has been established that the noise is mainly due to phase variations and that $a(t)$ is always very much smaller than unity.

Experiments, which we shall describe in this paper, have shown that the noise is predominantly due to microphony, to which tubes of this construction are particularly sensitive because of the presence of the two diaphragms (7). The extremely small vibrations of these diaphragms give rise to slight variations in the tuning frequency of both cavity resonators, resulting in phase variations and hence frequency variations of the output signal.

Another cause of noise, viz. fluctuations in the applied voltages, especially the anode voltage, can be kept very small by using adequately stabilized voltages.

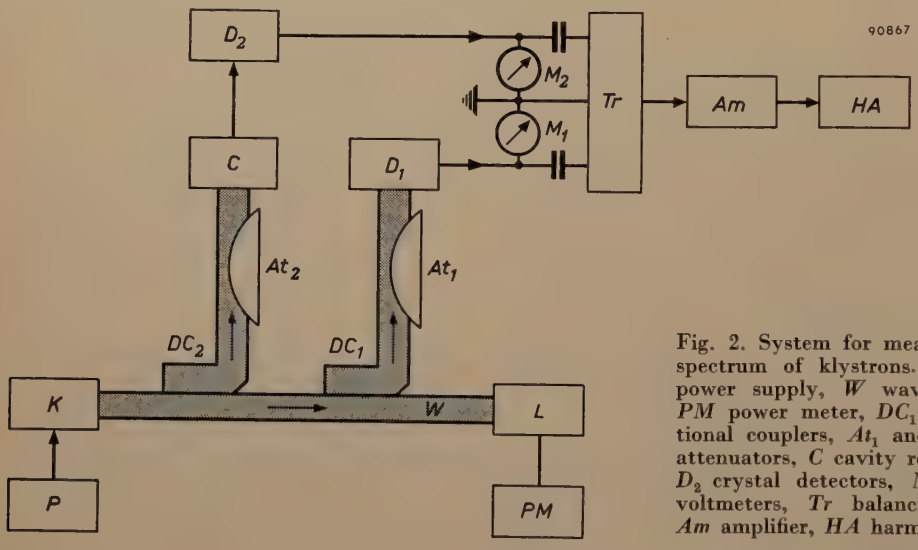

Fig. 2. System for measuring the noise spectrum of klystrons. K klystron, P power supply, W waveguide, L load, PM power meter, DC_1 and DC_2 directional couplers, At_1 and At_2 adjustable attenuators, C cavity resonator, D_1 and D_2 crystal detectors, M_1 and M_2 D.C. voltmeters, Tr balancing transformer, Am amplifier, HA harmonic analyser.

Noise measurements

Fig. 2 shows a block diagram of the system used for measuring the noise of klystrons. The tube K under investigation operates into a waveguide W terminated by a matched load L. Ignoring the slight losses in the waveguide, the output power of the klystron can be ascertained by measuring the power converted into heat in this load.

Two samples of the klystron output are "taken" from the waveguide W and directed into separate channels by two directional couplers[4]) DC_1 and DC_2.

The signal supplied by DC_1 is fed via an adjustable attenuator[4]), At_1, to a crystal detector D_1. Since the signal voltage appearing on this detector is very small, the output of the rectifier is proportional to the square of the signal voltage and therefore proportional to the output power of the klystron. This D.C. voltage, which contains a small A.C. component due to amplitude variations in the signal, can be read from meter M_1.

The signal from DC_2 is fed via a second adjustable attenuator, At_2, to a discriminator; this consists of a slightly detuned transmission cavity, C, to which a crystal detector, D_2, is coupled. The D.C. voltage from this detector can be read from meter M_2. As the discriminator detects fluctuations in amplitude as well as in frequency, the D.C. voltage output of this channel contains two A.C. components, one proportional to amplitude variations and the other to frequency variations in the klystron signal (there are also some small interaction terms present). When the D.C. outputs of both detectors are equal, the A.C. components in each output are also equal in so far as they are due to amplitude variations. The A.C. outputs from D_1 and D_2 are applied to a push-pull-transformer Tr in such a way that the voltage obtained in the secondary is mainly caused by frequency variations. This voltage is amplified in an audio amplifier Am and analysed by a harmonic analyser HA. From this voltage we can calculate the power spectrum of the klystron, the width of this spectrum being a measure for the noise.

A total of four klystrons of the type shown in fig. 1 were analysed in this way, with the results shown in *fig. 3*. Here we plot the power against the frequency, expressed in W per c/s. A measure for

[4]) See A. E. Pannenborg, A measuring arrangement for waveguides, Philips tech. Rev. **12**, 15-24, 1950/51.

the width of these spectra is the so-called standard deviation

$$\bar{\gamma} = \sqrt{\frac{\int_0^\infty x^2 S\,dx}{\int_0^\infty S\,dx}}.$$

For the curves shown in fig. 3 the value of γ lies between 3.3 and 12 kc/s.

The fact that the noise is mainly due to the microphony arising from the diaphragms was plainly demonstrated by the following experiment. After the spectrum of one of the tubes had been recorded, the diaphragms and tuner were cast in plaster of Paris, and the spectrum again recorded. The spectra before and after this treatment are represented as curves *a* and *b* in *fig. 4*. The root mean square deviation was reduced in this way from 5.3 to 1.9 kc/s. The plaster of Paris was then removed and the tube was cast in plastic, after which the spectrum was again recorded. The result is shown as curve *c* in fig. 4. The root mean square deviation was now found to be only 200 c/s.

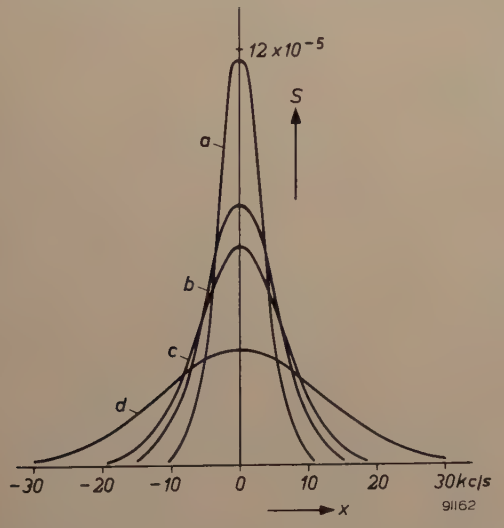

Fig. 3. Spectrum of four tunable klystrons, recorded with the layout shown in fig. 2. The power S, expressed in W per c/s, is set out along the ordinate; x is the frequency deviation from the central frequency of the spectrum.

Construction of a low-noise tube

The main source of the noise having been determined, various methods were considered for reducing microphony. Firstly attempts were made to build a more robust tuner to hold the diaphragms more firmly (see fig. 8), but the results showed very little improvement, the r.m.s. deviation of the tubes so constructed being of the order of 2 kc/s. As a low noise level was so important that the tuneability of the tube could if necessary be sacrificed for this purpose, it was furthermore considered to cast the tubes in plastic, after first tuning them to a specified frequency. It would also be possible to make tubes with only one diaphragm, i.e. with one of the cavities tuned to a fixed frequency, and finally a tube might be designed with no diaphragms at all.

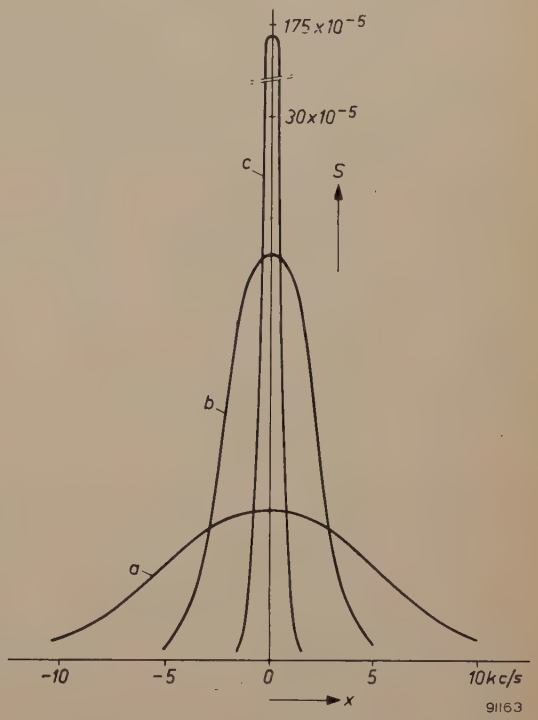

Fig. 4. Spectrum of a tunable klystron, *a* in normal state, *b* after casting in plaster of Paris, *c* after casting in plastic.

In that case a variable feedback coupling would be necessary to adjust the tube to the conditions for delivering its rated power. An important objection against the latter method lies in the fact that a variable feedback coupling would entail a complicated mechanism, which would very likely also cause microphony and, consequently, noise.

It was therefore finally decided to develop a tube without diaphragms and with a fixed feedback coupling. In spite of the absence of a diaphragm the output cavity can nevertheless be tuned. A simplified cross-section of this tube is shown in *fig. 5*. The modulating cavity *1* is permanently tuned to the desired resonant frequency. The output cavity *2* is adjusted, while the tube is oscillating, by applying to the collector a large force, denoted by the arrow *F*. This force is large enough to strain the cavity wall beyond its elastic limit. When this occurs, the cavity can be deformed to the right amount, at which it remains permanently set. As in the tube shown in fig. 1, the feedback coupling is effected via an opening *10* in the wall between the two cavities.

Characteristics of the low-noise tube

The cathode of the tube described here may be either an L cathode [2]) or an impregnated tungsten type [5]). The life of these cathodes is better than 1000 hours and, compared with tungsten, tungsten-thorium or tantalum cathodes, the heater power they require is low; in the present case it is only 7 W [6]).

The electrode *6* (fig. 5) with which the electron beam is focused, can be used for amplitude modulation and is therefore generally called the "grid".

As described in the articles quoted in [1]), a klystron can be made to operate in different modes, i.e. with different electron transit times between the modulating and output gaps. The tube under discussion can operate in three different modes, denoted by *A*, *B* and *C*, which correspond respectively to transit times of $2^3/_4$, $2^1/_4$ and $1^3/_4$ periods. The power delivered in these modes is respectively 5, 33 and 200 watts. Each klystron is adjusted to operate in only one of these modes and will not perform properly in other modes.

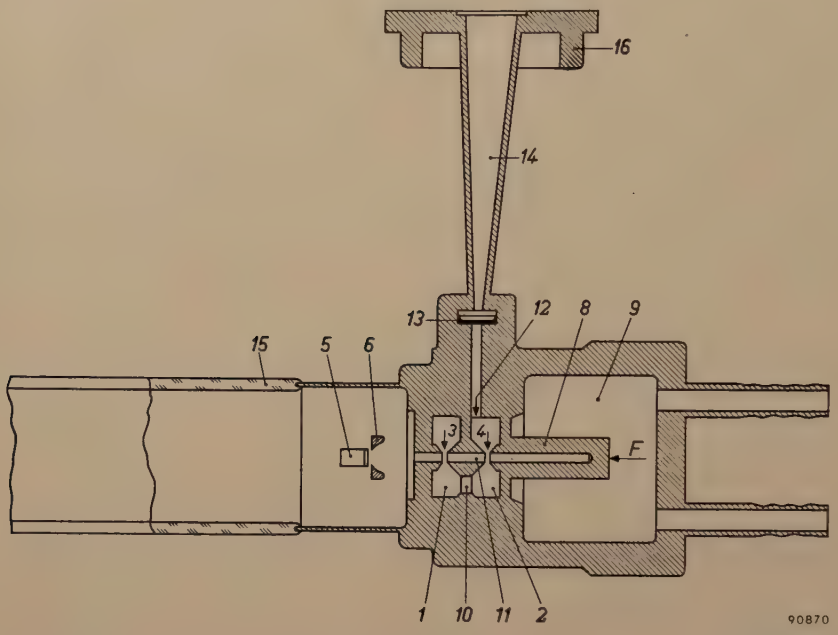

Fig. 5. Cross-section of a low-noise klystron. The figures have the same meaning as in fig. 1. *F* force required to tune the output cavity *2*.

By varying the "grid" voltage it is also possible to change the frequency between certain limits. At normal operating conditions this electrode has the same potential as the cathode.

The diode characteristic of the tube, i.e. the collector current plotted as a function of collector voltage, is shown in *fig. 6*. As for every diode, this characteristic can be represented by the equation:

$$I_c = AV_c^{3/2}.$$

In this tube the constant A (the perveance) is approximately 0.25×10^{-6} A/V$^{3/2}$. The tube is liquid-cooled and the maximum rate of flow required for water cooling is about 1/2 gallon per minute.

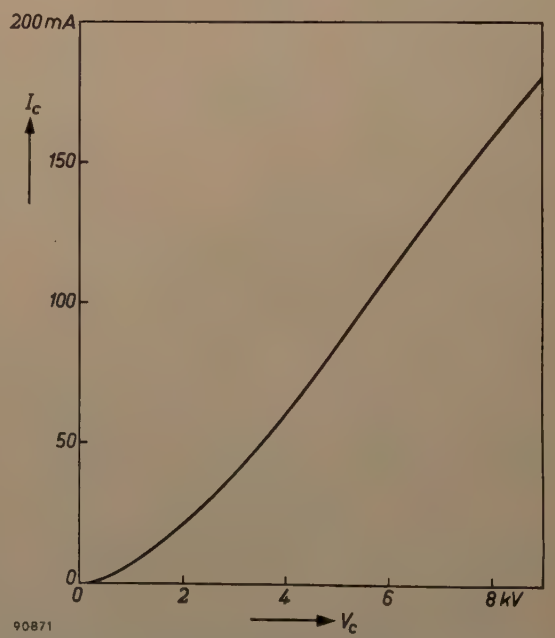

Fig. 6. Diode characteristic of a klystron as shown in fig. 5. I_c collector current, V_c collector voltage.

[5]) R. Levi, New dispenser type thermionic cathode, J. appl. Phys. **24**, 233, 1953. This cathode will shortly be discussed in full detail in this Review.

[6]) Oxide cathodes, which require an even lower heater power, cannot be used in these tubes because their useful life at the high emission needed would be only a few hours.

Tunable klystrons, as illustrated in fig. 1, do not deliver rated power output over their whole tuning range. This can be seen from the typical power versus frequency characteristic of a tunable tube, at two different modes, shown in *fig. 7*. The low-noise

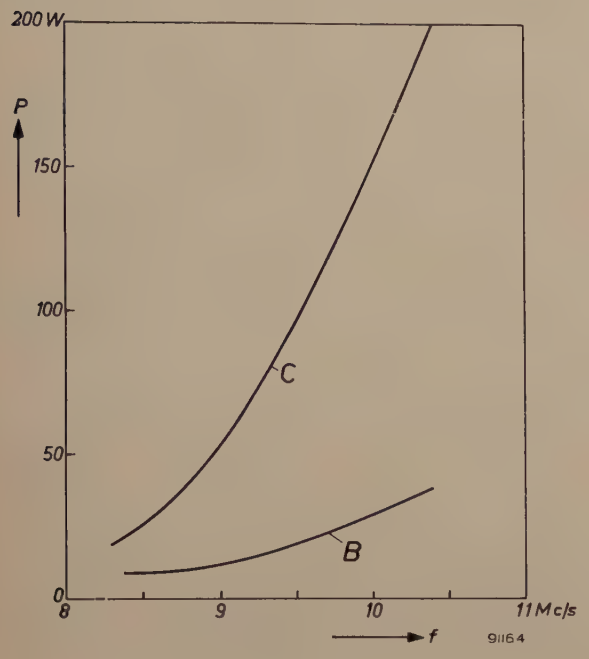

Fig. 7. Power output of a tunable klystron as a function of frequency for modes *B* and *C* (electron transit time $2^1/_4$ and $1^3/_4$ periods respectively).

tube, due to its method of manufacture, gives always its rated power. The frequency where this takes place, can (as indeed the most favourable frequency of a tunable klystron) be fixed at any desired frequency with a maximum error of 10 Mc/s.

The absence of a tuner makes the construction of this tube much simpler than that of tunable types. This is illustrated in *fig. 8*, in which are shown an older tunable klystron, a tube with "ruggedized" tuning mechanism and a non-tunable low-noise tube. Because of the remarkable precision with which the new tube can be made for any specified frequency, it is possible to switch over or interchange a series of such tubes for quickly altering a transmitter frequency. This would often be easier than tuning a normal klystron.

The noise of these tubes is so low that we were unable to measure the power spectrum with the system described. It appeared that the waveguides in the measuring system were now more microphonic than the klystrons under investigation.

The elimination of the diaphragms and tuner offers some advantages in addition to the substantial reduction of noise. In the first place it lowers the cost of the tube. Further, it allows more accurate alignment of the electrodes, while the absence of diaphragms leads to a somewhat better heat distribution.

Fig. 9 shows the results of some measurements of the variation of power output and frequency with collector voltage. The curves relate to modes *B* and *C* (mode *A* has been omitted because we are interested mainly in higher power outputs). The power is plotted on a normalized scale, obtained by dividing the power output by the maximum power delivered in each mode. This maximum power is 33 W for mode *B* and 200 W for mode *C*, at anode voltages of 4.35 and 8.85 kV respectively. The collector current and the efficiency do not differ much from those of a tunable tube.

The fact that the frequency variation curve reverses its direction is not in accordance with the theory of the electrical phenomena. The assumption that thermal effects in the tube are responsible

Fig. 8. From left to right: an early type of tunable klystron, a tunable klystron with ruggedized tuning mechanism and a low-noise, non-tunable klystron.

for this phenomenon was made and this was verified by two experiments. Temperature variations influencing the static curves in fig. 9 do not appear if the anode voltage is rapidly varied. For this reason the tube operating in mode *B* was "swept" in anode voltage at a rate of 60 c/s and the frequency variations measured through the mode. The result is represented by the dot-dash curve in fig. 9. A reversal of the frequency curve does not occur now.

In a second experiment a small AC voltage with a higher frequency was superimposed on the anode voltage, thus producing frequency modulation. From the spectrum of the output signal the frequency deviation per volt variation in collector potential was calculated. The result is shown in *fig. 10*, together with the power curve shown already in fig. 9. Whereas it would follow from the static frequency curve that, at a collector potential of about 3.9 kV, small voltage variations would give rise to no variations in frequency, i.e. the modulation sensitivity would be zero, experiment showed that the modulation sensitivity never becomes zero. In fact the frequency variation per volt follows quite closely the slope of the *dot-dash* curve in fig. 9.

The tube can also be modulated in amplitude by means of the grid voltage. *Fig. 11* shows, for modes *B* and *C*, the power in terms of the grid voltage. The latter voltage has also some influence on the frequency. The frequency variation has also been depicted in fig. 11. As this variation is principally due to changes in temperature, it is not possible to generate frequency-modulation in this way, but this phenomenon can be used for electronic tuning within a certain small frequency range. From fig. 11 it can be seen that the maximum frequency variation is much higher for mode *C* than for mode *B*.

The temperature of the coolant has some influence

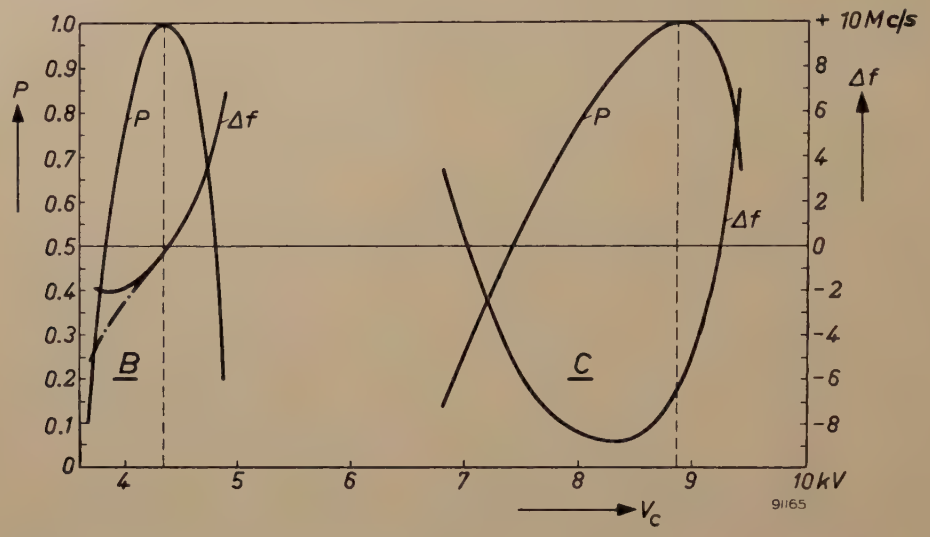

Fig. 9. Power output *P* and frequency variation Δf of a low-noise non-tunable klystron as shown in fig. 5, mode *B* on the left, mode *C* on the right. The power is plotted on a normalized scale. The maximum power for *B* is 33 W and for *C* 200 W. The fully-drawn curves are the results of static measurements. The dot-dash curve is the result of measurements in mode *B* with rapidly varying collector voltage.

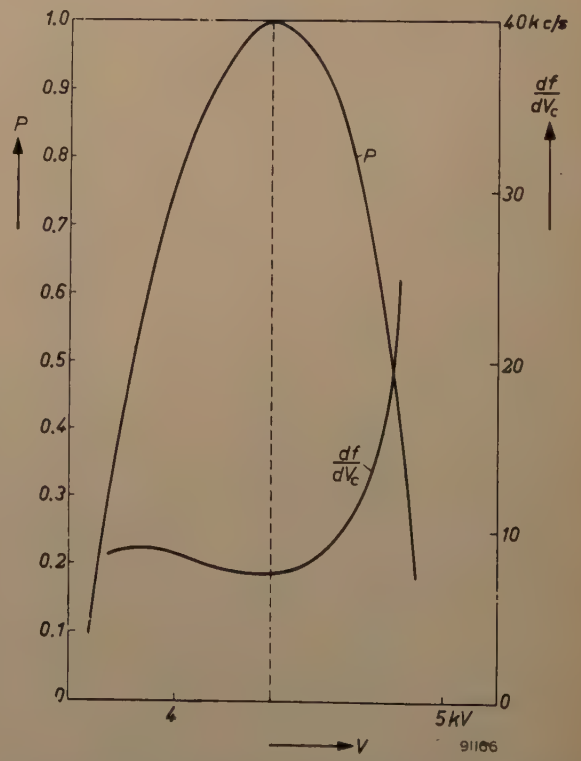

Fig. 10. Frequency variation per V variation in collector voltage, df/dV_c, as a function of the collector voltage in mode *B*. The power output *P* on a normalized scale is also shown; this curve corresponds to that shown on the left in fig. 9.

on the frequency. We found a frequency variation of 0.2 Mc/s per degree variation in temperature. Immediately after switching on, the frequency drift is approximately 2 Mc/s per second for a constant coolant temperature. After the warming-up period the effect of ambient temperature upon frequency is extremely slight.

A change in the load impedance affects the output power and also causes a frequency shift. A good impression of the tube's behaviour at different load impedances is given by a Rieke diagram, i.e. a polar diagram is which the modulus and the argument of the reflection coefficient of the load coupled to the waveguide are plotted [7]). In this diagram lines of constant power and lines of constant frequency shift are shown. A typical Rieke diagram for a tube operating in mode *B* is shown in *fig. 12a*, and a

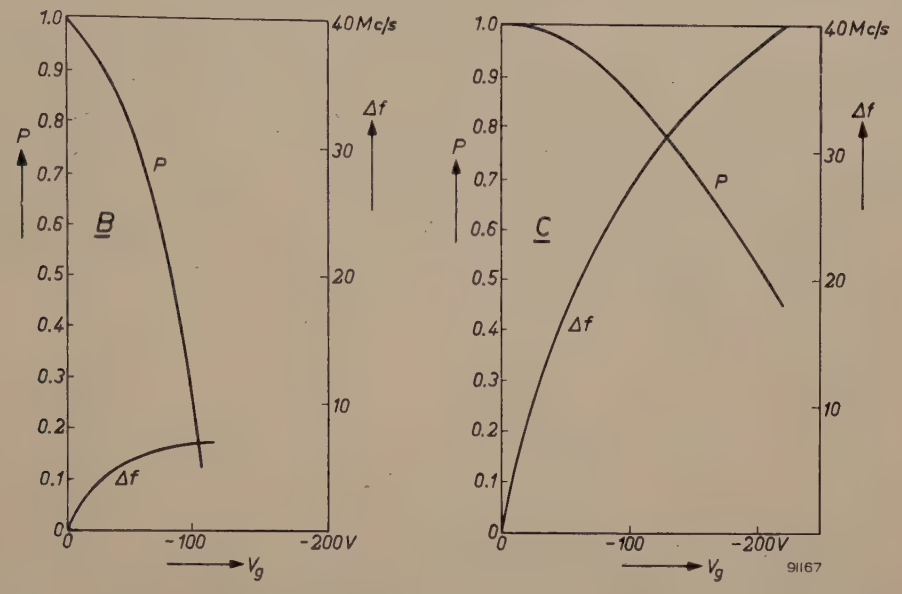

Fig. 11. Power output P and frequency variation Δf as functions of grid voltage. The power is set out on a normalized scale. The left curve refers to mode *B*, maximum power 33 W; the right curve refers to mode *C*, maximum power 200 W.

[7]) See e.g. D. R. Hamilton, J. K. Knipp and J. B. Horner Kuper, Klystrons and microwave triodes, Radiation Laboratory Series, No. 7, McGraw-Hill, New York 1948, Chapter 15.

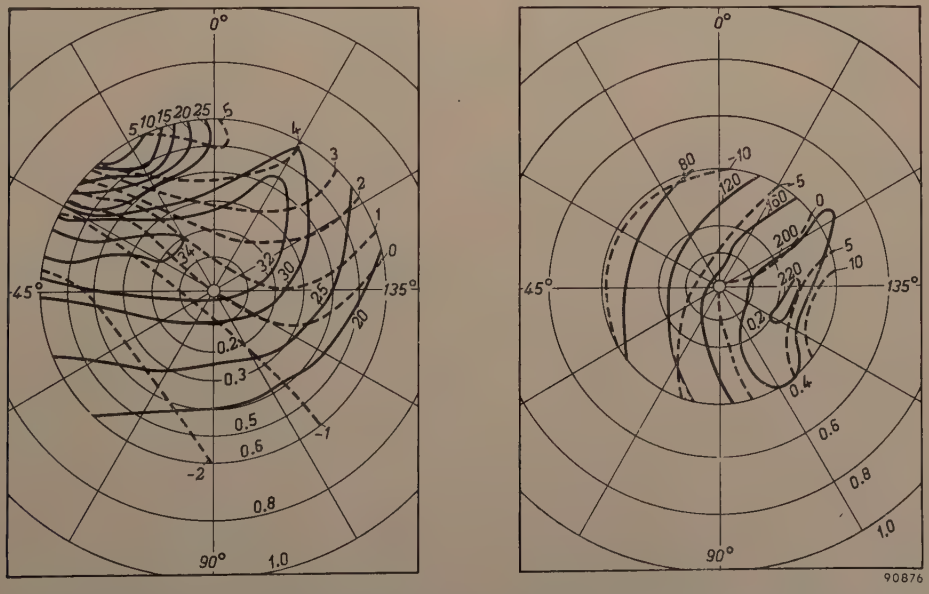

Fig. 12. Rieke diagrams for modes *B* (left) and *C* (right). The lines of constant power (in W) are fully-drawn; the dashed curves are lines of constant frequency deviation (in Mc/s).

Rieke diagram for a tube operating in mode C is shown in fig. 12*b*.

If the load impedance is varied such that the modulus of the reflection coefficient remains 0.2 while the argument passes through all angles between 0° and 360°, a certain frequency variation is produced which is known as the "pulling figure" of the tube. Fig. 12 shows that for modes B and C the pulling figures are about 4 and 9 Mc/s respectively.

Some tubes, namely magnetrons and some klystrons can be damaged when they are used with a load which is not that which gives the maximum power output. In many cases the window which ensures the vacuum-tight sealing is damaged. In this respect it is of some interest to mention that the tube described here has worked in mode B without difficulties with a load having a voltage-standing-wave ratio of 7. In mode C voltage-standing-wave ratios up to 5 have been used.

Summary. The flexible diaphragms with which most tunable klystrons are equipped are the most important source of noise in these tubes. Owing to the demand, in a certain application, for a tube with a much lower noise level, a non-tunable klystron has been developed in which these diaphragms are absent. This tube has a very much lower noise level. It can be used in three modes, delivering respectively 5 W, 33 W and 200 W. The tube can be frequency and amplitude modulated by variation of the collector voltage; amplitude modulation can also be effected by the grid voltage. Variation of the grid voltage also permits, via thermal effects, a certain limited tuning of the tube.

ULTRASONIC MACHINING

II. OPERATING CONDITIONS AND PERFORMANCE OF ULTRASONIC DRILLS

by E. A. NEPPIRAS*) and R. D. FOSKETT*).

534.321.9:621.95

Machining by means of ultrasonic vibrations is finding widening fields of application. Part I of this article gave an introduction to this technique and described some of the ultrasonic drills developed by the Mullard Research Laboratories. The present (concluding) article considers in some detail the factors which are important with regard to cutting speeds, accuracy and surface finish. A brief comparison is made with other special techniques, notably that of electro-erosion.

Cutting speed

The machining rates attainable with ultrasonic reciprocating tools are affected by many factors, apart from those quantities fixed by the constructional features of the vibrator — oscillatory amplitude, operating frequency and static loading — which have been briefly considered in Part I of this article [1]). The other factors include: the material of the tool; its shape; its area; the depth of the cut; the physical properties of the work material; and the abrasive properties including the hardness, grain dimensions, the nature of the suspension medium and the concentration of the suspension.

Drilling tests have been carried out under varying operating conditions, in an attempt to assess the effect of all these variables. It was found that with increase in the static load (L), cutting rates (penetration in inches per minute) always increase from zero almost linearly at first to a maximum at some optimum load and then decrease, the curve of cutting rate against L becoming asymptotic to the L axis (*figures 1a* and *b*). Increase of oscillatory amplitude ξ at fixed frequency has the effect of increasing cutting speeds and at the same time shifting the optimum load to higher values (see fig. 1*a*). It seems obvious that at least two separate effects contribute to the observed results — a damping effect which becomes important at high values of load, superimposed on a linear law of increase which predominates at low pressures. This becomes more apparent when we study the curves relating to tools of varying areas (fig. 1*b*). The optimum load increases with the tool area, the peak becomes broader, and for tools of very large areas the damping effect becomes unimportant over the range of loads used. For small-area

*) Mullard Research Laboratories, Salfords, Surrey, England.

1) E. A. Neppiras and R. D. Foskett, Ultrasonic machining, I. Technique and equipment, Philips tech. Rev. **18**, 325-334, 1956/57, hereafter referred to as I. Erratum to article I: in footnote [15]), the subscripts to k should read $\lambda/2$ and not $y/2$.

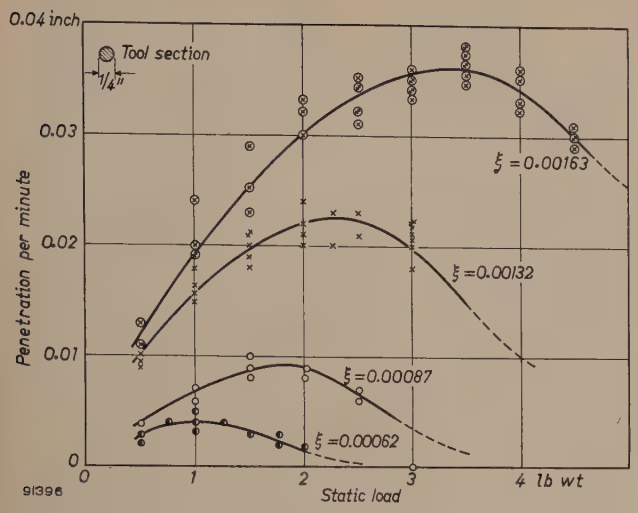

a

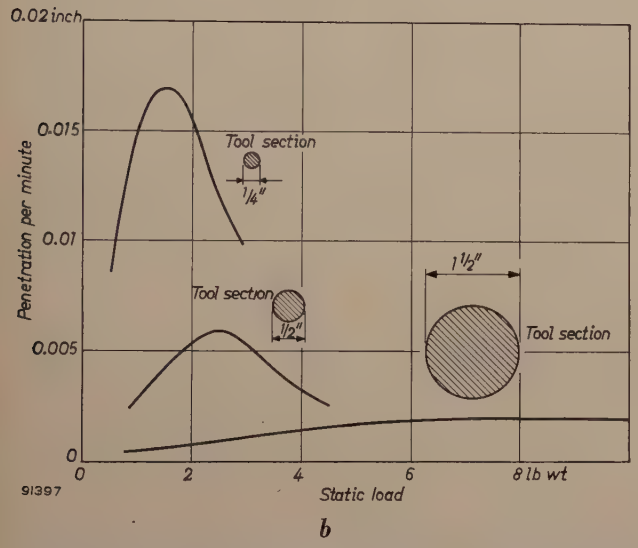

b

Fig. 1. *a*) Cutting speed (thousandths of an inch penetration per minute) as a function of static load for four different vibration amplitudes.
b) Cutting speed as a function of static load for tool sections of three different areas.

tools, the adjustment of the load for optimum working becomes more critical. Cutting rates are greater for tools of smaller area under otherwise identical conditions, but the increase is not by any means simply related to the cutting area. There is a much closer correlation between the cutting rate and the shape of the tool face — particularly the lateral dimensions when the tool face is long and narrow. This would be expected, the effect being mainly attributable to the difficulty of the abrasive grains penetrating to the centre of a large tool. It also seems that the optimum loading conditions are very dependent on the concentration of the abrasive which reaches the tool face.

The whole position in regard to cutting speeds is complex, but the effects are on the whole what might be expected from the simple mechanics of the process. An increase in the oscillatory amplitude ξ at constant frequency means a proportionate increase in particle velocity $\omega\xi$ and in the impulsive forces communicated to the work. The increased amplitude also means that a proportionately greater range of abrasive grain sizes are being brought into use in the grinding process. The cutting speeds would therefore be expected to increase at a rate more than proportional to ξ, as is indeed the case (*fig. 2a*). Under conditions of optimum loading, the law is often approximately quadratic. Wide divergencies from this rule occur only when L does not approximate to the optimum value and in cases where the peak-to-peak oscillatory amplitude of the tool differs considerably from the grain dimensions of the abrasive (see also footnote [8]) in I).

The optimum value of external applied load would also be expected to increase with increase in ξ.

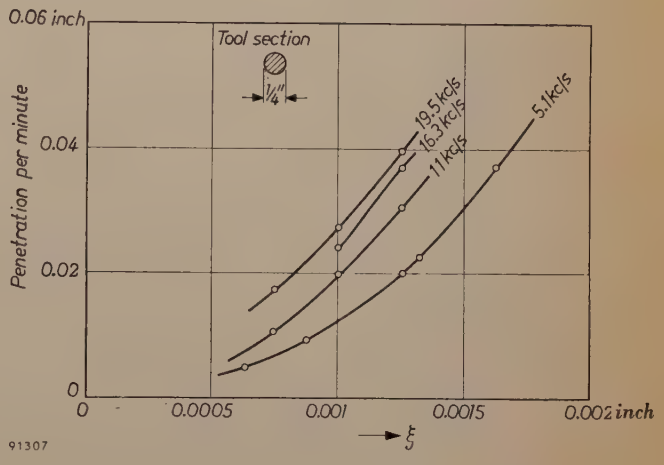

a

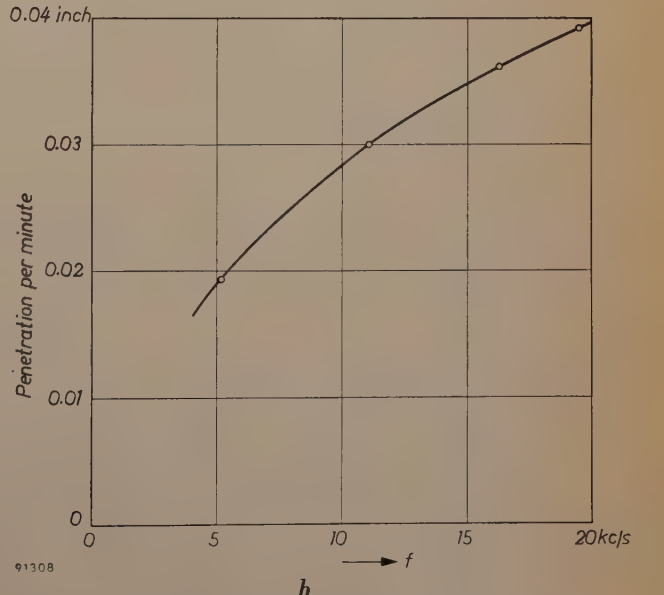

b

Fig. 2. Cutting rates in glass *a*) as a function of oscillatory amplitude (peak-to-peak) of the tool face, and *b*) as a function of the frequency, for a fixed amplitude of 0.00125″ peak-to-peak. These graphs (*a*) and (*b*) are reproduced from figs. 1 and 2 of part I.

These predictions take no account of complications which may be introduced due to difficulties of abrasive circulation. Nevertheless, they are well borne out in practice.

In the absence of complicating effects, cutting rates would be expected to increase as the square of the operating frequency at constant amplitude, since the impulse delivered at each impact and the number of blows per second are both proportional to the frequency. Over the range of frequencies 5 to 20 kc/s, however, cutting rates were found to increase slowly with frequency at a rate rather less than linear (fig. 2*b*), the variation being apparently independent of both oscillatory amplitude and abrasive grit size. This increase is much smaller than would be expected from theoretical considerations. The observations cover the range of frequencies normally used for piezomagnetic transducers. Measurements using other types of vibrator at frequencies around 100 c/s, however, have shown that at these low frequencies the square law relationship between cutting speeds and frequency does hold precisely. The complete curve relating cutting speed with frequency therefore contains a point of inflexion. Beyond this point the *overall* efficiency drops and there is therefore a theoretical optimum working frequency near this point. However, this would not necessarily be an ideal value to use in practice, since several other practical considerations enter into the choice of operating frequency.

A series of measurements of cutting speeds carried out using tools formed in various common metals of widely different physical properties showed that cutting speeds are not greatly dependent on the tool material; figures for cutting speeds in glass and sintered tungsten carbide, relative to various tool materials are given in *Table I*.

An advantage is generally gained by using trepanning tools in roughing operations, except where the overall dimensions are small and the hole deep. When tools of very complex section are used, so that the total area of tool surface wall in contact with the liquid is large, considerable viscous damping is imposed on the sides of the tool and this increases with the depth of penetration. For very deep holes the tool should preferably be retracted at regular intervals to achieve an efficient removal of abraded material and help abrasive circulation.

Cutting rates generally increase with increase in grit size of the abrasive powder but only provided the lateral dimensions of the tool are everywhere large compared with the grain dimension. Some typical curves, all referring to the same tool, are shown in *fig. 3*. There is also a significant correlation between the optimum abrasive grit size and both the oscillatory amplitude of the tool and the static

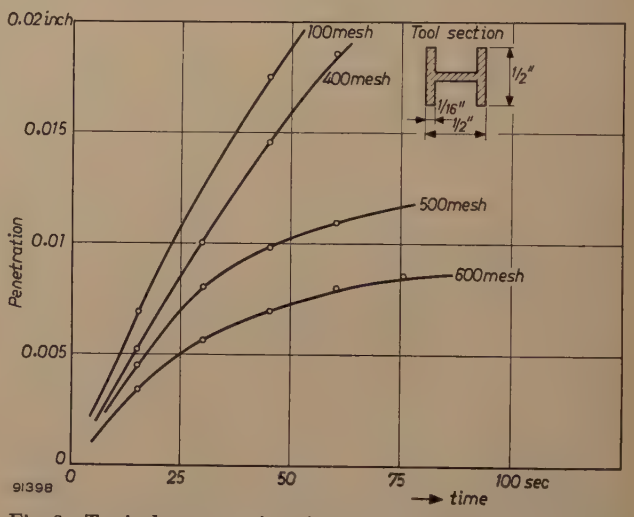

Fig. 3. Typical penetration-time curves showing the effect of abrasive grain size on cutting speed. Grain size is given in terms of British Standard sieves.

Table I. Dependence of cutting speeds on the material of the tool. Cutting rates averaged over about 0.1 inch penetration. (Abrasive: boron carbide; material: soda glass; optimum static load.)

Tool material	Tool shape	Cutting rates, thou'/minute, for			
		$\xi = 0.002''$		$\xi = 0.001''$	
		Abrasive 100 mesh	Abrasive 400 mesh	Abrasive 100 mesh	Abrasive 400 mesh
Copper	Circular, $^1/_8''$ diam.	63	20	16	6
Brass (BSS 251)	,,	90	28	22	8
Mild steel (EN2)	,,	86	22	21	7
Silver steel*)	,,	74	22	20	8
Stainless steel (18% Cr, 8% Ni, 0.1% C)	,,	71	20	18	6
Tungsten carbide	Triangular, base = $^1/_8''$	156	100	38	30
Mild steel (EN2)	,,	150	102	36	29

*) C 0.87%, S 0.020%, P 0.025%, Mn 0.28%; tempered in air after oil-quenching from 800 °C.

Table II. Comparative cutting speeds in industrial ceramics (soda glass, using 100 mesh B_4C abrasive, = 100; tool: mild steel, circular, diam. $^1/_4$″).

Work material	Abrasive					
	Boron carbide		Silicon carbide			Alumina
	100 mesh	400 mesh	100 mesh	400 mesh	600 mesh	220 mesh
Chemical porcelain	70	14	53.5	11	2	25
"Temperadex" *)	60	10	45	7.5	—	20
"Faradex" *)	55	7	41	5	—	2
"Vulcanex" *)	190	51	168	44	2	62
Z.Z. porcelain	90	32.5	75	26	2	10
H.T. porcelain	45	24	41	22	—	8
"Frequentite" *)	47.5	27.5	45	26	—	20
Soda glass	100	45	80	37	6	70

*) Trade names of proprietary materials.

load. It seems to be an advantage to keep the grain dimensions comparable with the peak-to-peak oscillatory amplitude, at any rate when coarse abrasives are used. There is also a very significant variation of cutting speeds with the depth of the cut, as may be seen in fig. 3, and this also involves changes in the optimum static loading conditions and grit sizes.

Measurements of cutting speeds have been carried out in a wide range of materials of widely different physical properties using various abrasives with a a wide range of grit sizes. The results, listed in *Tables II-IV*, show cutting speeds relative to that in soda glass. They show that, in all cases, the drilling rates depend on the hardness of the abrasive used — cutting rates are always greater with boron carbide than with silicon carbide of the same grit size, and greater with SiC than with alumina. This is rather surprising since hardness is not the only physical property of importance. The shape of the abrasive grains (the number of cutting edges) and their ability to withstand fracture are obviouslv important factors, It might be thought that in materials which are sufficiently soft relative to these abrasives, the hardness of the abrasive should cease to be important and relative cutting rates would then be determined by the secondary factors

Table III. Comparative cutting speeds in metals. (Tool H-form, $^1/_2$″ square, limbs $^1/_{16}$″ thick, see fig. 3; soda glass, using 100 mesh B_4C abrasive, = 100.) The figures in brackets in Tables III and IV are estimates, interpolated from measurements under somewhat different conditions from those stated above.

Material	Abrasive						
	Boron carbide			Silicon carbide 100 mesh	Alumina 220 mesh	Sand (grit size 0.012″)	Diamond powder (grit size 0.001″)
	100 mesh	220 mesh	400 mesh				
Soda glass	100	90	77	85	65	47	90
Brass (common yellow)	6.6	5.6					
Die steels							
(i) K.E. 672 (R. 66)	1.4	1.3					
(ii) C.S.K. (R. 62)	3.9	3.6					
(iii) K.E. 672 (R. 61)	2.2	2.1		1.48	0.1	0.1	
(iv) K.E. 672 (R. 58)		1.7					
Stainless steels							
(i) 18% Cr, 8% Ni, 0.1% C	2.1	1.9					
(ii) 3.5% Cr, 8.4% W, 0.35% V, 0.3% C	1.2	1.1					
Carbon-chrome bearing steel (heat-treated)	1.4						
Sintered tungsten carbide (R. 76)	4.1	3.5		2.55	0.2	0.2	4.3
Tungsten	4.8	4.3					
"Stellite"	4.0	3.7					
Germanium single crystal	(31)			(28)			
Titanium	(4.0)						
Beryllium	(7)						

Table IV. Comparative cutting speeds in various brittle materials. (Tool H-form, $^1/_2''$ square, limbs $^1/_{16}''$ thick, see fig. 3; soda glass, using 100 mesh B_4C abrasive, = 100.)

Material	Abrasive			
	Boron carbide			Silicon carbide
	100 mesh	200 mesh	400 mesh	100 mesh
Soda glass	100	90	77	85
"Hysil"	73	66	54	
B9 borosilicate glass	86			
Ferroxcube IIIC	37			34
Ferroxdure (demagnetized)	(32)			
Quartz crystal	(57)			
Fused alumina	19			
Synthetic sapphire	19			
Synthetic ruby	18			
Flint stone	(72)			
Barium-titanate ceramic	110			109
Ceramic 507	(38)			35
Carnet	(58)			
Felspar	(40)			
Spinel	(48)			
Slate	67			
"Mycalex"	(240)			(200)

mentioned above. If this was the case, silicon carbide would provide the fastest rates. If hardness is really the most important physical property of the abrasive determining cutting rates it should be possible to use an ultrasonic machining test to grade abrasives in a reliable scale of hardnesses. A soft brittle material would be used as a standard sample test piece. Taking soda glass as a very brittle and comparatively soft material, the figures given in the tables rank boron carbide, silicon carbide and alumina in the order 100 : 80 : 72. The Knoop hardness figures for these abrasives are 2250, 2100 and 1650 (100 : 93 : 73).

From a study of the data in Tables II, III and IV, it is clear that brittleness is the most important single property of the workpiece which determines its machinability. (For the present purpose brittleness is taken to mean the ability to chip pieces up to 0.001 inch in size from the workpiece.) It should be noticed that many materials which are ductile and malleable at ordinary temperatures, and therefore not easily machined ultrasonically, become brittle when the temperature is reduced sufficiently, so that the technique in fact possesses a considerably wider potential field of application than might be thought from the measurements recorded here which, of course, all refer to normal room temperature.

It will be seen that cutting rates are greatest for glasses and certain ceramics. In metals, with the exception of germanium, speeds are lower, generally by a factor of some 25-100. However, even in tough hard metals not noted for their brittleness, cutting speeds are generally high enough to make the ultrasonic technique industrially interesting.

Experience has shown that the most convenient method of feeding the abrasive to the tool in practical drilling operations, particularly when long jobs are involved, is to operate a continuous circulation system, employing a considerable volume of slurry so that only infrequent bulk changes of the abrasive are necessary. When the abrasive is fed externally to the tool it is pumped on to the work from one or more jets; for large areas it is essential to use several jets to ensure an even circulation of abrasive in the cut. In deep holes a fast continouos jet feed generally produces rather faster cutting rates as compared with manual feed, since the jet aids the abrasive circulation. An alternative method of applying the abrasive to the work, which overcomes the difficulties encountered in deep drilling operations, is to force-feed the abrasive suspension through the tool itself. This has been found a very valuable technique but it is of course only applicable to trepanning operations.

For efficient operation, the usable concentration of the abrasive is limited by the ability of the mixture to flow easily under the tool and by the danger of a very concentrated suspension drying out. The optimum concentration will vary with the working conditions, abrasive grain size and suspension medium but as a general guide it should form a paste of syrupy consistency. Typical curves showing the variation of cutting speed with abrasive concentration are given in *fig. 4*.

In deciding the best type of liquid to use as the carrying medium for the abrasive, the indications are that a low viscosity is a desirable property, particularly in piercing operations, since the abrasive suspension must flow in a restricted path and the intensity of cavitation (on which depends the efficiency of abrasive circulation) is also a function of the viscosity of the medium. The liquid should also have good wetting properties with respect to the work material, the tool, and the abrasive; it should presumably also have a high density, approaching that of the abrasive (in order to retain it in suspension) and, for efficient cooling, a high thermal conductivity and specific heat. Experimental work carried out using a wide range of available liquids as carrying media for the abrasive has largely verified these ideas. Water, with or without small additions of surface activating agents,

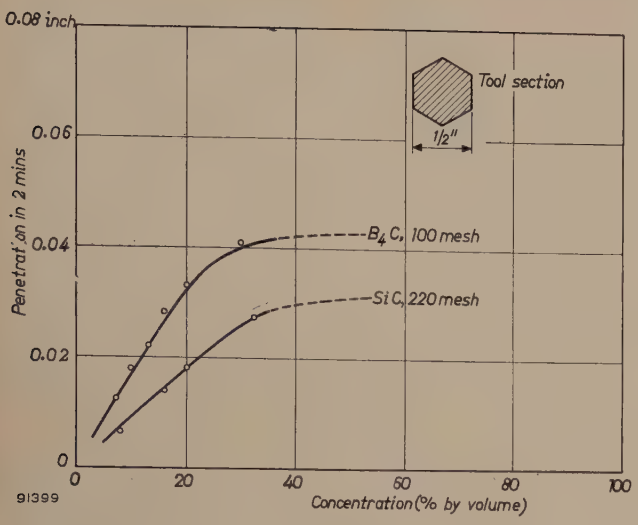

Fig. 4. Cutting speed in glass, as a function of abrasive suspension concentration, for two different abrasives.

is about the best liquid available and far more satisfactory than most oils, even thin oils.

Measurements have also been made of the wear produced in the tool (see *Table V*) under similar conditions to those noted in Table I. Of the materials tested the relative wear is least in the case of silver steel. It seems that, for minimum wear, a hard tough steel is desirable. Whether, in any particular case, the advantage to be gained in using a material of this sort rather than a softer steel is likely to outweigh the disadvantage resulting from the greater difficulty in fabricating the tool is another question. Tools of copper and similar very soft metals are definitely not suitable for piercing work, not because wear is excessive or that cutting speeds are slow, but because plastic deformation of the tool at high vibration intensities causes distortion of the tool face (mushrooming).

To conclude this section, the following specific example may be quoted for the cutting rate obtained in machining a typical shaped hole in a brittle material: Using a spline trepanning tool of mild steel, about $\frac{1}{2}$ inch diameter, similar to that shown in the photograph of fig. 11 in I, a hole was cut through $\frac{1}{4}$ inch thick sintered tungsten carbide in about 42 minutes. In this operation the peak-to-peak oscillatory amplitude of the tool was 0.0025 inch, 220 mesh boron carbide powder in water was used as abrasive and the static loading was adjusted to about the optimum value, $3\frac{1}{2}$ lbs. wt.

Table V. Tool wear. (Abrasive: boron carbide 100 mesh; $\xi = 0.002''$; optimum static load.)

Tool material	Tool shape	Work material: Glass — Longitudinal tool wear (inches)	Glass — Total penetration in workpiece (inches)	Glass — Tool wear as % of stock removal	Work material: Tungsten carbide — Longitudinal tool wear (inches)	Tungsten carbide — Total penetration in workpiece (inches)	Tungsten carbide — Tool wear as % of stock removal
(a)							
Copper	Circular, $\frac{1}{2}''$ diam.	0.0025	0.520	0.48	—	—	—
Mild steel (EN2)	,,	0.018	1.850	1.0	0.110	0.125	88
Silver steel *)	,,	0.0025	0.546	0.46	0.012	0.046	26
Stainless steel (18% Cr, 8% Ni, 0.1% C)	,,	0.008	1.150	0.7	0.016	0.045	35
Brass (BSS 251)	,,	0.021	1.250	1.68	0.175	0.125	140
Sintered tungsten carbide	Triangular, base = $\frac{1}{8}''$	0.0015	1.510	0.1	0.138	0.125	110
		Tool steel			Tungsten carbide		
(b)							
Mild steel	Circular, hollow, int. diam. = $\frac{1}{8}''$, ext. diam. = $\frac{1}{4}''$				0.156	0.125	125
Mild steel	H-form, $\frac{1}{2}''$ square, limbs $\frac{1}{16}''$ thick	0.053	0.024	220			
Mild steel	Circular, hollow, int. diam. = 0.33", ext. diam. = 0.39"				0.170	0.075	222
Brass	Extrusion shape T-form, height of T = 16 mm				0.256 (average)	0.125	205

*) C 0.87%, S 0.020% P 0.025%. Mn 0.28%; tempered in air after oil-quenching from 800 °C.

The work on cutting speeds reported above refers to piercing operations. In lapping and repassing work in which the wearing is produced essentially by frictional action, the position is much simpler. Difficulties due to abrasive circulation and complications concerning the relation between abrasive grit dimensions and tool size, oscillatory amplitude and penetration, do not arise. Also, experience shows that in this type of operation there is no optimum static load related to the other variables. Provided that the cutting is done essentially by frictional forces, cutting rates increase continually with the applied load, until a point is reached when the tool tends to stick in the hole and the flow of abrasive is impeded. In all operations of this sort, it is a great advantage to retract the tool at intervals to allow a better flow of abrasive between tool and work. If this is not done, the maximum usable load may be very small in deep holes, unless the oscillatory amplitude is much greater than the abrasive grain dimensions.

An important advantage of the high frequency machining technique is that under normal operating conditions it leaves no residual mechanical stresses in the material which is being cut. This is shown by the fact that even in the most brittly easily-fractured materials, the pieces chipped off in the machining process are small compared with the abrasive grit dimensions, showing that the stresses communicated to the workpiece are extremely localized even though the particle acceleration of the tool is generally very great. (The acceleration $\omega^2\xi$ is, for example, about 25 000 g for a frequency of 16 kc/s and a peak-to-peak amplitude of $\sim 0.002''$.)

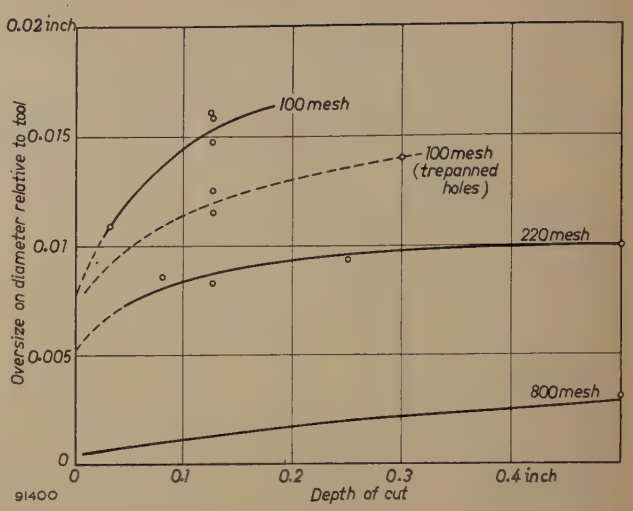

a

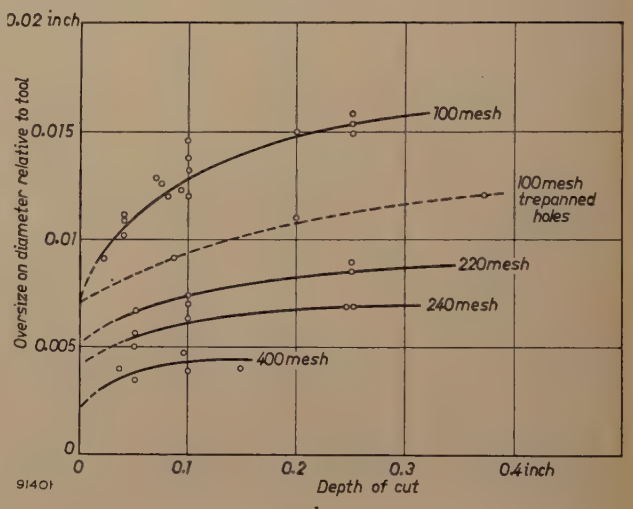

b

Fig. 5. Oversize on diameter as a function of depth of cut, for various abrasive grain sizes, *a*) in tungsten carbide, *b*) in soda glass. Abrasive in both cases was boron carbide.

Accuracy

Since the abrasive grains must necessarily pass down the sides to get under the tool, the resulting hole is oversized relative to the tool, the oversize being greater at the entry and getting progressively less towards the exit for through holes. When close dimensional tolerances are required it must be possible to predict the oversize quantitatively.

The variations of oversize with the depth of the cut and grit size of abrasive, under approximately optimum load conditions, have been measured and are shown in *figs. 5a* and *b*. The oversize on radius is initially always a little greater than the lower limit of the grit dimensions of the abrasive. The oversize at the entry increases rapidly, as the hole becomes deeper, to a value which corresponds fairly well to the upper limit of the grit dimensions. Thereafter the increase is comparatively slow, being a function of both penetration and time, and relatively greater for the smaller grit sizes. The oversize is seen to be a little greater in tungsten carbide than in glass for the same depth of cut, showing that the ratio of lateral to longitudinal wear is greater in the former case.

Measurements show that drilled *blind* holes are always tapered towards the bottom in such a way that the oversize at the bottom is only of the order of the smallest of the abrasive grains present in the suspension. This means that probably few of the larger grains ever reach the fool face in such a drilling operation.

Apart from the abrasive, other factors contributing to the oversize obtained are those relating to the precision of the mechanical arrangements: 1) the accuracy with which the transformers and tools are aligned with respect to the transducer, 2) the accuracy with which the slide mechanism allows motion

of the drill in a vertical direction only, and 3) the relative perpendicular alignment of the drill and the worktable. Deficiencies in 1) and 3) will result in the tool entering the work in a slanting direction so that the hole drilled out by a circular tool will show ovality of an amount depending on the depth of penetration.

Since cutting rates are so much greater when coarse abrasives are used, while good surface finish and close dimensional tolerances both demand fine grit size, the drilling operation must be performed in several stages when very accurately dimensioned holes are required. A hole is first drilled through using an undersized tool of dimensions which can be estimated from a knowledge of the depth of the cut and grain size of the abrasive to be used. Then a second repassing or sizing operation is carried out, for which the tool will be cut only slightly undersize, a fine abrasive being used, the precise grit size depending on the surface finish required. The repassing process will be rapid since if the roughing operation has been correctly carried out it will be necessary to remove only a very small volume of material. When great accuracy is required, or very deep holes to a reasonable tolerance, the hole can be drilled in three operations, the final one being done with a close tolerance tool and a polishing grade of abrasive, such as 2000 mesh.

The order of dimensional accuracy obtainable in single-stage drilling operations is such that, even when using coarse (220 mesh) abrasive powder, the dimensions of the cut can be predicted to within about ± 0.002 inch if a tool is used which is considerably longer than the hole depth. (The tool will then follow through after penetration and remove, by lapping, inaccuracies due to tool wear.) For many applications this degree of precision may be sufficient. For two-stage drilling operations, the dimensional accuracy achieved in glass and tungsten carbide, using 800 mesh repassing powder, can be better than ± 0.0005 inch.

To illustrate the accuracy obtainable by ultrasonic machining in the important field of die making, two typical examples will be described. The first of these is a gauge in tungsten carbide designed to check splined shafts. The shaft cross section and that of the gauge are shown in *figs 6a* and *b*; the gauge is also illustrated in the photograph of fig. 6*c*. The drilling was carried out as a 3-stage operation. A circular hole was first cut in the blank, using a trepanning tool and a roughing grade of boron carbide. The diameter of the hole obtained by this operation was approximately 0.015 inch less than the required 0.530 inch root diameter of the finished gauge. A solid splined tool having the shape of the required finished hole but 0.005 inches undersize was next used in a second roughing operation. The resulting hole was approximately 0.0015 inches radially undersize relative to the required dimensions. The work was now considered ready for finishing and a final tool 0.0005 inches undersize was used together with a fine grade of boron carbide.

The second example to be described, a blanking die for valve anodes, is illustrated in *figs. 7a* and *b*. The die was cut from a $\frac{1}{8}$ inch (3 mm) thick tungsten carbide plate. In this case, one roughing cut was followed by two finishing operations. The tools were made successively 0.010, 0.004 and 0.001 inch undersize on all internal linear dimensions and were brazed on to cylindrical brass half wave

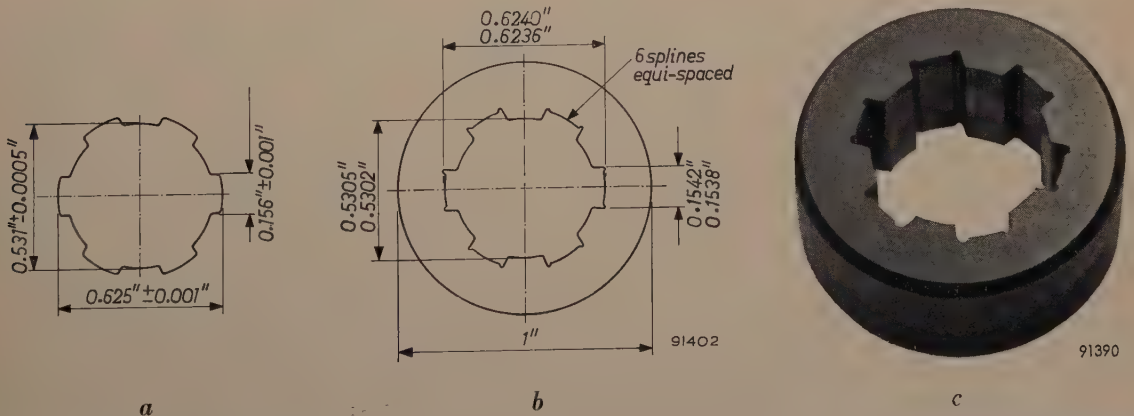

Fig. 6. *a*) Cross-sections of splined shaft. *b*) Dimensions of tungsten carbide ("no-go") gauge. *c*) Photograph of finished gauge.

stubs. In order to make use of the slight taper obtained in a normal drilling operation, the work was so arranged that the face clamped to the work table should become the upper face of the die. By a final lapping operation using the largest tool and 800 mesh abrasive, the die was brought very

accurately to size so that it was just possible to press the punch through by hand. The resultant clearance between punch and die was very small — of the order of 0.0003 inch. Sections of the die wall taken after each ultrasonic operation are shown in fig. 7*c*. These show clearly the dimensional accuracy obtained in the operation.

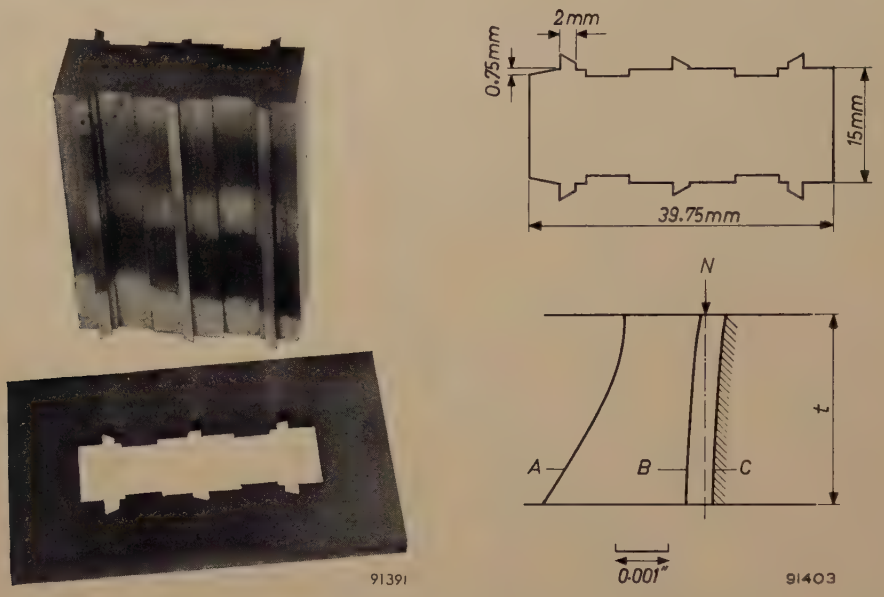

Fig. 7. *a*) and *b*) Photograph and sketch of tungsten-carbide blanking die for valve anodes. *c*) Contours of the die wall, *A* after roughing out, *B* after second operation and *C* after the final ultrasonic machining operation. *N* shows the specified nominal size. The thickness *t* of the die is drawn on a much smaller scale than that used for the horizontal distances.

To summarize we may say that the order of dimensional accuracy depends only on the two factors mentioned above — the abrasive grit size and the mechanical precision inherent in the mounting assembly — and is not restricted by any basic limitation imposed by the technique itself. With regard to the precision of the mounting, the two main problems are 1) ensuring that the drilling tool is fixed with its axis parallel to the line of movement of the drill head or the work; 2) aligning a tool for a finishing operation with the cut already produced by a roughing tool. Both these questions, which are closely related, are being investigated.

Even for cutting circular dies, the vibration technique possesses a considerable advantage in speed over conventional methods. In such cases, both the cutting speeds and circularity of the die hole can be improved by rotating the die at a slow constant rate during the drilling. The essentials of a rotatable die holder used for the production of tungsten carbide wire-drawing dies are shown in the sketch of *fig. 8*. The die blank is supported centrally in a circular metal container carrying the abrasive suspension. The die holder carries holes at the base to allow the continuous circulation of abrasive through the die hole. The tool is supported on the die with the appropriate static load and the container rotated at a slow rate (about once every 5 seconds). The abrasive is circulated either manually or by means of a fixed vane dipping into the slurry.

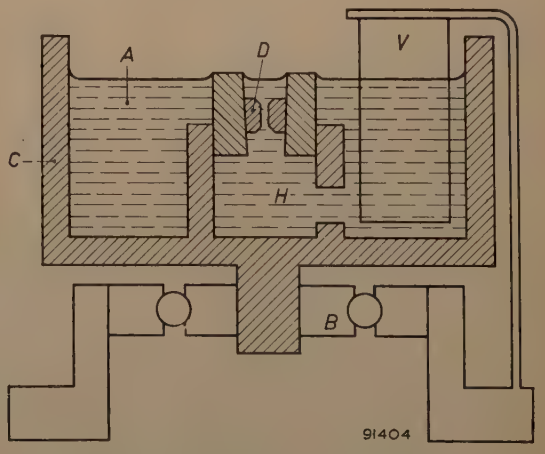

Fig. 8. Mechanical set-up for the ultrasonic drilling of tungsten carbide wire-drawing dies. *A* abrasive suspension, *B* bearing, *C* rotatable metal container, *D* die blank, *V* sloping vane to aid stirring of abrasive, *H* holes in die holder to provide path for abrasive circulation.

Surface finish

Measurements have been made of the quality of the surfaced finish obtained on the bottoms and sides of roughed and repassed holes in glass and tungsten carbide. These measurements were carried out with the aid of a Talysurf roughness tester which plots a trace of the surface irregularities and records a centre-line average figure for the roughness height over the final 0.3 inch of surface examined. The following general conclusions can be drawn from all the measurements recorded.

The quality of the surface finish is closely related to the abrasive grit size as shown clearly in the four traces of *fig. 9* referring to 100, 400, 600 and 800 mesh boron carbide powders, the measurements being taken at the bottom of blind holes drilled out under approximately optimum drilling conditions. For the coarse abrasives the peak-to-peak irregularities sometimes amount to as much as 0.001 inch; for the fine powders they are never more than about 0.0001 inch. Trace (*d*) is interesting in that it shows what appears to be a small cavitation channelling mark. These are rarely found at the bottom of blind holes.

with abrasive flow. Increasing the load results in a reduction in the size of abrasive grains which can reach the tool face. Consequently, when coarse abrasives are used the roughness height on the sides of blind holes is greater than at the bottoms.

The roughness height does depend somewhat on the oscillatory amplitude of the tool: it increases slowly with amplitude under optimum drilling conditions.

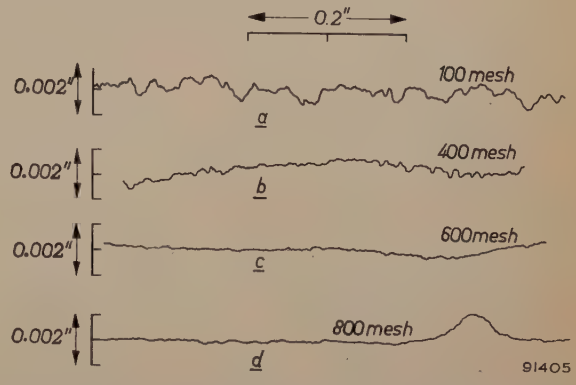

Fig. 9. Surface traces over the bottoms of blind holes in glass, bored with boron-carbide abrasives. (Talysurf roughness tester. Note difference in vertical and horizontal scales.)

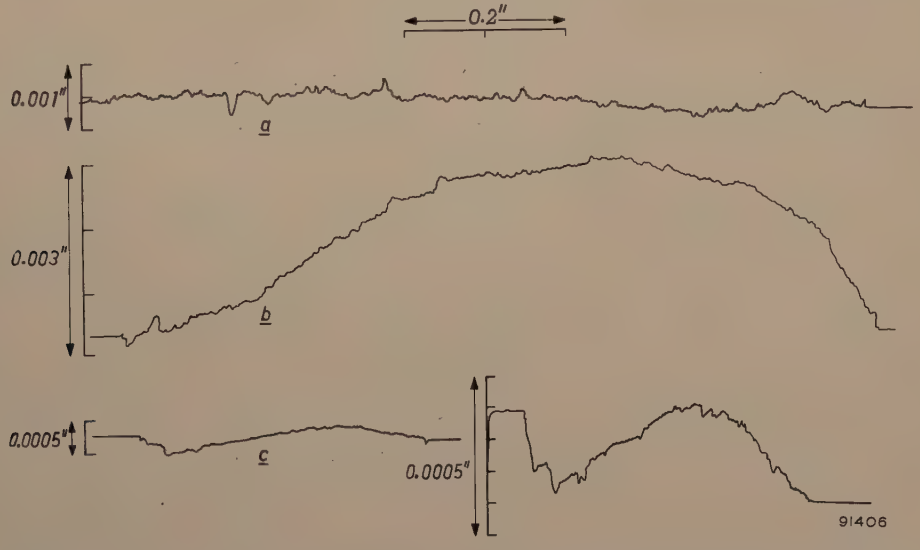

Fig. 10. Surface traces for blind holes in tungsten carbide, bored with boron-carbide abrasives.
a) Bottom of surface cut, tool penetration 0.005″; 100 mesh abrasive.
b) Bottom of hole 0.1″ deep, 100 mesh abrasive.
c) Side of repassed hole, 800 mesh abrasive. The trace on the right refers to the same region as that on the left, but is on a 5× enlarged scale.

The quality of the surface finish appears to be quite independent of the static loading conditions. This is a rather surprising result; it might be expected that the roughness height should increase approximately linearly with the applied load in the same way as cutting speed. The explanation appears to be that there is a compensating effect associated

The traces of *fig. 10* refer to cuts in tungsten carbide. Traces (*a*) and (*b*) refer to the bottom of blind holes, using 100 mesh boron carbide abrasive (amplitude = 0.002 inch, under approximately optimum operating conditions). (*a*) is for a surface cut, the tool having penetrated only about 0.005 inch. The surface irregularities are greater than in

(*b*), a similar trace for a hole 0.1 inch deep. This is an indication that when the abrasive circulation depends on the motion of cavitation streamers (viz. when hole depth $\gg$ clearance between tool and work, i.e. $\gg$ abrasive grain size), the largest grains never reach the tool face. In (*b*) the large-scale modulation of the trace represents a surface undulation caused by irregular tool wear. Trace (*c*) refers to the side of a repassed hole in a tungsten carbide slab, using 800 mesh boron carbide powder.

Fig. 11 shows a plot of the measured surface roughness height as a function of the abrasive grit size in glass and tungsten carbide. In piercing operations the roughness height at the sides is of the same order as that obtained at the bottom except when the coarsest abrasives are used. In repassing operations, for all practical purposes the surface finish can be taken to be dependent only on the grit size of the abrasive and independent of the oscillatory amplitude and static load. Under the same operating conditions, the roughness heights in glass and tungsten carbide (bottoms of holes) are approximately in the ratio 7 : 1, although cutting speeds are about in the ratio 24 : 1. The surface traces show clearly that stock removal occurs essentially by a chipping action in both glass and carbide.

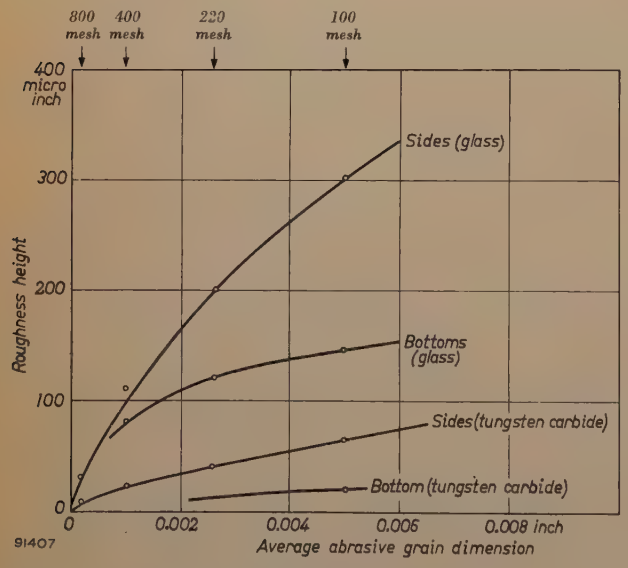

Fig. 11. Surface roughness height as a function of abrasive size for holes in glass and tungsten carbide.

The quality of the surface finish obtained on the sides of holes is sometimes by no means uniform. The rougher patches consist of channels cut into the surface of the material by the action of cavitation streamers drawing abrasive grains between the tool and the work. These markings have already been referred to in Part I of this article (see also fig. 9*d* above). Their nature is shown clearly in the micrograph of *fig. 12*. The width and depth of the channels seem to be related to both the grain size of the abrasive and the width of the streamers themselves. With coarse abrasive the depth of the channels is about the order of the grain dimensions, and although they become shallower for finer abrasives they are rarely less than a few thousandths of an inch in width and depth. As already stated in I these markings can be prevented from forming by carrying out the machining operation sufficiently rapidly: the cavitation streamers are then unable to form a stable pattern and wear due to this cause is thereby distributed randomly over the surface.

Fig. 12. Micrograph showing cavitation markings on the surface of a cut in tungsten carbide.

Comparison with other techniques

Tools based on ultrasonic vibrators have rendered possible new types of machining operations, jobs which had not previously been attempted on account of their extreme difficulty or tediousness. In some of its potential uses, however, the technique is in competition with other methods. This is true of most applications relating to metals, including the fruitful field of die-making. Apart from sintering followed by hand-lapping techniques, there are other more efficient modern processes now being applied to this problem of the accurate machining of complex shapes in hardened steels and carbide. These include the various spark and electro-arcing techniques.

Briefly, the ultrasonic machining technique is characterised by rapid cutting rates combined with the comparative ease with which accuracy and extremely good surface finishes can be achieved. No heat is generated in the work and consequently no changes are introduced in the physical structure of the material. The equipment is safe to handle and requires skilled labour only in making and

setting of the actual tools; these are, however, cheaply made in a comparatively soft metal. Cheap abrasives are used and expensive diamond bort is needed only for drilling diamond. It is also important to notice that the technique is applicable to all brittle materials and is not limited by any other physical property of the substance. Extreme hardness of the work material does not constitute a limitation to its machinability, but it is, of course, necessary to choose an abrasive which is as hard or preferably appreciably harder.

For forming irregular-shaped holes and depressions, patternmaking and multiple cutting in brittle materials, we can say that applied to non-conducting substances the vibration technique virtually has no competitor. When applied to conducting materials on the other hand the ultrasonic method is in competition with the new electro-erosion processes. The chief competitor to vibration machining techniques is the "electrosparking" process [2]) developed commercially in a number of countries, including America, Britain, Switzerland, Czechoslovakia and Russia. Fundamentally the process depends on producing very high localised instantaneous charge densities at the surface of the workpiece by initiating a succession of spark discharges across the space between the tool and workpiece, this being filled with a non-conducting liquid. In this process the spark erosion produces saucer-shaped depressions in the surface of the workpiece which are larger the greater the energy of the spark, so that the quality of the surface finish is in inverse ratio to the cutting speed. Although the method is capable of extremely high cutting speeds, greater than at present can be achieved by the vibration technique, it is not possible to rapidly achieve a good quality finish. It seems that to obtain even a reasonably good finish it is necessary to perform the machining in several successive operations, of which the final one may be an extremely lengthy process. The ultrasonic method is not limited in this way, a reasonably good finish being obtained even in roughing operations. For this reason it has been suggested that it may be possible to combine the two techniques, using the spark machine for roughing where any considerable bulk of material is to be removed and the ultrasonic abrasive process for finishing. Some experiments have been carried out in this direction with encouraging results.

Both these new machining techniques are still very much in the development stages and it is too early to attempt a rigid assessment of their comparative value. It seems that to a great extent the techniques are complementary rather than competitive even when applied to conducting materials, while for non-conductors the ultrasonic method has no serious competitor.

Summary. This second article on ultrasonic machining deals in some detail with cutting speeds, accuracy and surface finish. The various factors affecting cutting speeds are considered with the help of graphs and tables. Cutting speeds increase almost linearly with static load until an optimum value (dependent on vibration amplitude and frequency) is reached. For tools of small area the adjustment to optimum load is critical. Within the range of usable amplitudes and at ultrasonic frequencies, cutting rates increase rather more than proportionally with amplitude and rather less than proportionally with frequency. Cutting speeds are higher with coarser abrasives up to a grain size limited by the vibration amplitude. Considerable data is given of actual cutting speeds in various metals and brittle materials (glass, ceramics, minerals, etc) using different abrasives of various grain sizes. Cutting speeds vary from a few thousandths of an inch to some tenths of an inch per minute according to the work material, abrasive, tool material, etc. Tool wear is also discussed briefly. The effect on accuracy of abrasive grain size and mechanical precision of the drill mounting are discussed. Two examples are given illustrating the accuracy obtainable (of the order of $\pm$ 0.0005″). Surface finish and its relation to abrasive grain size and vibration amplitude is also discussed. Ultrasonic machining has no competitor where hard non-conducting materials are concerned; for conducting materials it is less rapid than some electro-erosion techniques but is capable of higher accuracy and smoother finish.

[2]) See for example I. Koncz, Electric spark machining, Gépész (Hungary) **1**, 388-411, Sept.-Oct., 1949 (abbreviated translation in Engrs. Digest (London) **11**, 108-111 and 165-168, 1950); also D. W. Rudorff and H. Drubba, Research (London) **7**, 216-220, 1954.

CATHODE-RAY DISPLAY OF COMPLEX QUANTITIES AT VARYING FREQUENCIES

621.317.34:621.317.755

It is often required to know precisely how a complex physical quantity behaves throughout a certain range of frequencies. Examples of such quantities are:

1) The complex ratio of input voltage or current to output voltage or current in electrical four-poles such as amplifiers, band pass filters and transistors, the ratio being expressed by a polar phase-amplitude diagram or Nyquist curve [1]).
2) The complex ratio of input voltage to input current, or *vice versa*, at a terminal pair of an electrical or electro-mechanical two-pole or multi-pole.

As examples of electro-mechanical two-poles, mention may be made of electro-acoustic transducers such as piezo-electric and piezomagnetic vibrators [2]); it is mainly in the vicinity of their mechanical resonances that the behaviour of these devices is of interest.

To make rapid but nevertheless reasonably accurate determinations of complex quantities at various frequencies, we have developed an apparatus which automatically gives a picture of the complex vector diagram, for an adjustable frequency range, on the screen of a cathode ray tube [3]), this being in fact a television picture tube. Until now a bridge method has had to be used for determining the complex impedance or admittance diagram of an ultrasonic crystal vibrator — to give one example — and this method means determining the diagram point by point. The procedure takes many hours, during which various quantities have to be kept strictly constant. The new method allows the diagram to be made visible in a few seconds, and it indicates immediately how the diagram changes when something is modified in the electrical network or the acoustic load of the test object.

The new method is partly based on the principle described in the article named in footnote [1]). Three versions of the apparatus have so far been developed (they are not being manufactured), for ranges of test frequencies of 300-20 000 c/s, 15-1500 kc/s and 0.1-10 Mc/s. The frequencies quoted in the explanatory account that follows relate to the 15-1500 kc/s version, a photograph of which appears in *fig. 1*.

Fig. 1. Apparatus for the display of the complex ratio between currents and voltages at varying frequencies. The polar diagram is traced on the screen of a CRT having a long-persistence phosphor. The object under test seen on the table is a piezo-magnetic vibrator (pre-magnetized ferroxcube core with winding). The apparatus shown is suitable for test frequencies from 15 to 1500 kc/s.

[1]) See for example G. Thirup, An instrument for measuring complex voltage ratios in the frequency range 1-100 Mc/s, Philips tech. Rev. **14**, 102-114, 1952/53.

[2]) C. M. van der Burgt, Ferroxcube materials for piezomagnetic vibrators, Philips tech. Rev. **18**, 285-298, 1956/57.

[3]) After this article had been written a paper by E. C. Pyatt (J. Brit. Instn. Rad. Engrs. **16**, 563-567, 1956) came to our notice in which a similar type of instrument is described. Its relative frequency range is smaller, however, and it does not function automatically.

In the block diagram of *fig. 2*, Q_1 and Q_2 are crystal-controlled oscillators generating fixed frequencies of $f_{Q1} = 8505$ kc/s and $f_{Q2} = 8500$ kc/s. The voltages from Q_1 and Q_2 are fed to mixer stages M_1 and M_2 respectively.

Oscillator O_v supplies a frequency f_v which is variable between 8520 and 10 005 kc/s. The voltage from O_v is also fed to the mixer stages via buffer circuits B_1 and B_2, these being isolating stages to prevent feedback. Now, we want to obtain from the two signals it mixes, providing this stronger signal keeps within certain limits.

Mixer stage M_1 delivers a signal of frequency $f_v - f_{Q1}$ (= 15-1500 kc/s) which we shall call f_s, the signal or test frequency. Amplifier A_1 amplifies and passes on this signal to X, the apparatus under test, which might be an amplifier, a filter, a crystal vibrator or the like. Mixer stage M_2 delivers a signal of frequency $f_v - f_{Q2}$, which is amplified by A_2. This auxiliary frequency f_a is always 5 kc/s

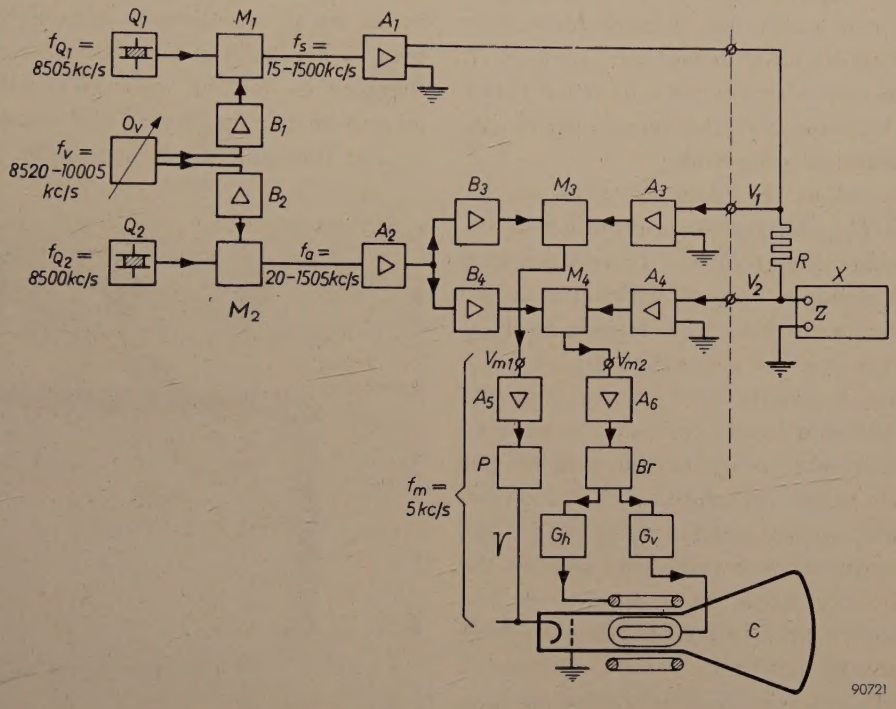

Fig. 2. Block diagram of the apparatus designed for a signal frequency range of 15-1500 kc/s. Q_1 and Q_2: quartz-controlled oscillators. O_v: oscillator of adjustable frequency f_v. B_1, B_2, B_3 and B_4 denote buffer circuits, M_1, M_2, M_3 and M_4 mixer stages, and A_1, A_2, A_3, A_4, A_5 and A_6 amplifiers. P: pulse-shaper. Br is a bridge circuit, one output voltage of which has a 45° lead and the other a 45° lag with respect to the voltage on its input. G_h and G_v generators of the deflecting currents for cathode-ray tube C. X test object. R series resistor used when the impedance Z of test object X has to be measured ($R \gg |Z|$, $Z \propto V_2/V_1$).

$f_v - f_{Q1} = f_s$, the test or signal frequency. $f_v - f_{Q2} = f_a$, the auxiliary frequency. $f_a - f_s = f_m$, the intermediate frequency, equal to 5 kc/s.

The voltage delivered by A_1 can be varied from zero to 1.5 V. The cable connecting A_1 and X has a characteristic impedance of 135 Ω (this being the internal resistance of A_1). In order that the pulse from P should be sufficiently strong, V_1 must be approx. 5 mV. It is necessary that V_2 should have the same value if the circle on the screen is to have a radius of 10 cm.

these mixer stages a signal whose amplitude is as nearly constant as possible, but the voltage from oscillator O_v inevitably varies rather considerably with the frequency f_v. This being so, it has been arranged that the buffer circuits deliver a voltage considerably higher than the constant voltages from Q_1 and Q_2; the reason for this is that the conversion transconductance of a mixer tube is more or less independent of the amplitude of the stronger of higher than f_s, for the difference between f_{Q1} and f_{Q2} is 5 kc/s. We shall call this constant difference frequency f_m, the intermediate frequency.

From the test object X two voltages V_1 and V_2 are obtained that are in phase with and proportional in amplitude to the quantities whose complex ratio has to be measured. (In fig. 2 it is assumed that an impedance Z is to be measured. A resistance $R \gg |Z|$ is connected in series with Z, so that the

resulting current is practically independent of the impedance. V_2 is the voltage across Z; V_1 is the voltage across $R + Z$ and is therefore a measure of the current through them.) Voltages V_1 and V_2 are fed to the mixer stages M_3 and M_4 respectively via amplifiers A_3 and A_4. The two voltages are mixed with a signal coming from amplifier A_2 via the buffer circuits B_3 and B_4. This auxiliary signal has the frequency f_a which, as stated above, exceeds the test frequency f_s of V_1 and V_2 by the constant amount of $f_m = 5$ kc/s. The mixer stages produce two voltages V_{m1} and V_{m2} having the intermediate frequency. As can easily be demonstrated (see page 103 of the article cited in footnote [1])), *these i.f. voltages have the same complex ratio as the h.f. voltages V_1 and V_2*, provided the mixer stages M_3 and M_4 have identical properties.

Continuing to follow the block diagram, we see that i.f. voltage V_{m2}, having been amplified in A_6, is applied to bridge circuit Br and there converted into two equal voltages, one of which has a 45° lag and the other a 45° lead with respect to V_{m2}. The two voltages control generators G_h and G_v, which supply the horizontal and vertical currents for magnetic deflection in the cathode ray tube C. The deflecting currents are sinusoidal and 90° out of phase. A circle would therefore be traced on the screen of the tube, were it not for the fact that the grid voltage is adjusted to a value such that in the normal state the electron beam is suppressed. The radius of the circle is proportional to the amplitude of V_{m2}, and hence to that of V_2.

The voltage V_{m1} is amplified in A_5; by clipping its peaks and differentiating it, pulse-shaper P turns the amplified voltage V_{m1} into a pulse train. The pulse train controls the cathode ray tube in such a way that the beam suppression is lifted intermittently: a point on the circle then becomes visible. Since voltages V_{m1} and V_{m2} have the same frequency (namely $f_m = 5$ kc/s), one point of the circle becomes visible on the screen. Which point becomes visible depends on the phase difference between V_{m1} and V_{m2}, and hence on the phase difference φ between V_1 and V_2. The radius of the circle (i.e. the distance from the visible point to the centre) is a measure of the ratio between the amplitudes of V_1 and V_2. Phase angle and radius can be read off on a grid of polar coordinates in front of the screen of the CRT.

As long as the frequency f_v of oscillator O_v is constant, the test frequency f_s has a fixed value and only one point of the vector diagram will be seen on the screen. If f_v is changed, f_s changes too, and the complex ratio being investigated generally takes on a different value, and consequently a point of a different circle appears on the screen. If f_s is made to pass through a certain range of frequencies the spot will trace out a curve representing the value of the complex quantity throughout that particular frequency range.

As a rule, the first stage in the measurement of a complex quantity is to cause f_s to pass from its lowest to its highest value by slowly varying f_v *by manual adjustment*. It is then easy to see from the screen values of f_s (read on an instrument scale) at which any interesting phenomena occur. Resonance shows up as an ellipse or a circle such as may be seen in *fig. 3*. Even two resonances occurring close together — one of which is easily overlooked in measurements employing the usual bridge methods — are immediately recognizable.

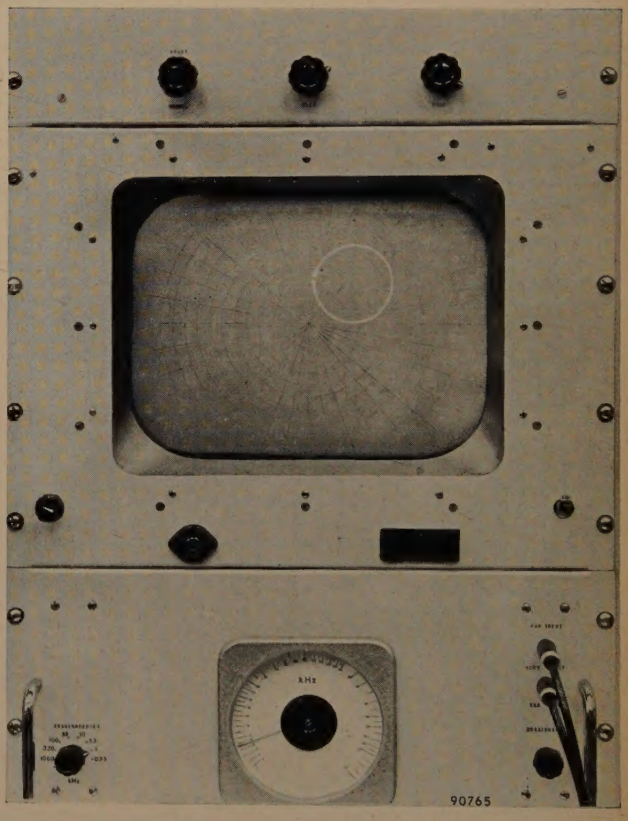

Fig. 3. On the screen can be seen one of the resonance circles of a piezomagnetic vibrator, occurring at a test frequency of about 35 kc/s. On the lower panel (left) is the control by which f_v (and hence f_s and f_a) is varied; f_s can be read off on the frequency scale (centre).

If it is desired to give closer study to the behaviour of the test object in the vicinity of such a frequency, an arrangement is put into operation that causes frequency f_s to swing about the set value by an adjustable amount and in an adjustable tempo. For this purpose use is made of the fact that the reversible permeability (i.e. the permeability in

relation to weak alternating fields) of ferroxcube almost saturated by a static magnetic field is dependent on the strength of that field. Part of the inductance in oscillator O_v is wound on a ferroxcube core; this is pre-magnetized by a direct current, and on this direct current an alternating current of adjustable amplitude and adjustable low frequency can be superimposed. In this way periodic fluctuation is set up in the reversible permeability of the ferroxcube core, and consequently in the frequency f_v, and in frequencies f_s and f_a as a further consequence. The sweep of f_s increases in accordance with the amplitude of the superimposed alternating current. The sharper the resonance of the test object (i.e. the higher its Q), the slower must be the rhythm in which f_s changes, in order that spurious responses near resonance be avoided. For the same reproducibility of the diagram and for the same frequency sweep (the width of the frequency range to be investigated is often determined by quantities other than the Q) the rate at which f_s fluctuates must be made inversely proportional to the *square* of Q. The maximum rate of swing is in fact proportional to $(f_s/Q)^2$, as has been demonstrated by Siewert and Just [4]). The apparatus for a test frequency range of 15-1500 kc/s can be used for Q values up to about 1000 at 15 kc/s and for proportionally higher Q values at higher frequencies. In this version of the instrument the frequency sweep (i.e. the maximum deviation from the central frequency) is adjustable in steps from 0.15 to 500 kc/s and the frequency of the superimposed alternating current (and hence the recurrence frequency of the screen image) is adjustable in steps from $^1/_{30}$ to 10 c/s. On account of this very low recurrence frequency, the CRT has a screen with a long-persistence phosphor.

The oscillograph method permits the measurement of complex quantities with an accurancy of within 5%. This means that the *true* end of the vector representing the complex quantity lies within a radius of 0.5 cm from the *observed* point when the vector has the maximum length of 10 cm. Hence the modulus can be measured with an accuracy of within 5% and the phase angle with an accuracy of within $^1/_{20}$ radian, or approx. 3°, for a full-scale reading. For smaller readings both modulus and phase angle are given with proportionally less accuracy.

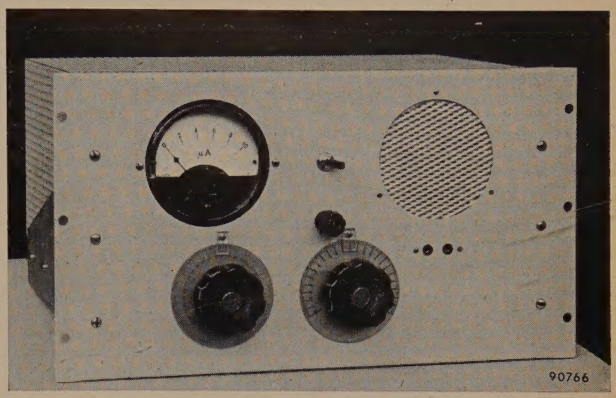

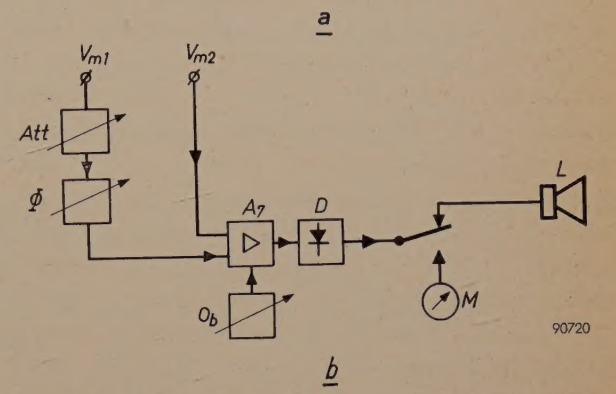

Fig. 4. *a*) Auxiliary unit with the aid of which the oscillograph method can be replaced by a null method [1]), should greater accuracy be required. *b*) Block diagram of the auxiliary unit shown in (*a*). *Att:* calibrated attenuator. *Φ*: calibrated phase-shifter. A_7: amplifier. O_b: beat oscillator. *D*: detector. Either meter *M* or loudspeaker *L* can be used for null indication. For the I.F. voltages V_{m1} and V_{m2}, refer to fig. 2.

If higher accuracy is desired, use can be made of the method described in the article cited in footnote [1]), and the auxiliary unit shown in *fig. 4a* added to the apparatus. In this way the oscillograph method is replaced by a null method. The block diagram of the auxiliary unit appears in fig. 4*b*. From the I.F. voltage V_{m1} a voltage is derived that is made equal in amplitude and phase to V_{m2} by means of a calibrated attenuator and a calibrated phase shifter. Equality between the two voltages is detected with the aid of an amplifier, a beat oscillator, a detector and some form of null-indicator. This last may be a meter or a loudspeaker. This method makes it possible to measure a modulus with an accuracy of within 0.2 dB (2%) and a phase difference with an accuracy of within 2°, *irrespective of amplitude*, provided this is not too low.

M. J. van SCHAGEN.

[4]) W. Siewert and G. Just, Ein Kurvenschreiber für Quarzimpedanzen, Telefunken Zeitung **28**, 45-51, 1955.

ABSTRACTS OF RECENT SCIENTIFIC PUBLICATIONS BY THE STAFF OF N.V. PHILIPS' GLOEILAMPENFABRIEKEN

Reprints of these papers not marked with an asterisk * can be obtained free of charge upon application to Philips Electrical Ltd., Century House, Shaftesbury Avenue, London W.C. 2.

R 306: H. G. van Bueren: Influence of lattice defects on the electrical properties of cold-worked metals (Philips Res. Rep. **12**, 1-45, 1957).

The first chapter of this thesis contains a review of the physical properties of dislocations, vacancies and interstitial atoms in the face-centred cubic metals copper, silver and gold. The mechanism of plastic deformation of such metals is then considered theoretically in order to obtain numerical data on the concentrations of the various imperfections present in the metal after cold-work. Measurements of electrical resistivity of slightly deformed copper and silver wires are presented and compared with the theory, thereby throwing light on several details of the deformation mechanism. By measuring the magnetoresistance of the strained wires, it is possible to separate the influences of dislocations from that of point imperfections. This, combined with observations of the thermal recovery of electrical conductivity after cold-work, a recovery characterized by four separate recovery stages, yields information on the diffusive as well as on the electron-scattering properties of the three types of lattice imperfections.

R 307: J. Haantjes and G. J. Lubben: Errors of magnetic deflection, I. (Philips Res. Rep. **12**, 46-68, 1957).

This paper deals with the errors caused by magnetic deflection of the electron beam in a cathode-ray tube. It appears that image distortion, astigmatism, curvature of the image field and coma may occur, corresponding to the errors of the third order in conventional optics. It will be shown that in most cases one may influence and even eliminate these errors by a suitable distribution of the deflecting field. The only error which can never be eliminated by a special field distribution is the error known as curvature of the image field. This error would not appear if the screen face of the tube coincided with the image field. However, the curvature of the image field is such that it is generally impossible to fulfil this condition. Therefore this error has to be taken into account in the design of cathode-ray tubes for television purposes.

R 308: K. F. Niessen: Spontaneous magnetization and magnetic susceptibilities of an antiferromagnetic with foreign ions in both sublattices (Philips Res. Rep. **12**, 69-81, 1957).

The spontaneous magnetization is calculated as a function of the temperature for an antiferromagnetic, in the two sublattices of which a different but relatively small number of original ions are assumed to be replaced by ions of another metal, carrying another magnetic moment. For a real calculation the Néel temperature of the material must be measured and also the Néel temperature of the original antiferromagnetic (in which the above replacement has not yet taken place). From the ingredients used for the preparation of the material the sum of the foreign ions in the two sublattices will be known, but not their ratio. This ratio, however, can be derived as a function of the temperature from the spontaneous magnetization. Moreover, we determine the change in the parallel and perpendicular susceptibilities, due to the above replacement of original by foreign ions.

R 309: B. H. Schultz: Storage of injected carriers at surfaces of germanium (Philips Res. Rep. **12**, 82-96, 1957).

The relative number of particles at the surface in the presence of an injection is calculated with the aid of standard space-charge theory. The effect of this "surface storage" on the relaxation of photoconductance is discussed. Measurements have been made of τ_{rel} of thin n and p type germanium rods as a function of their thickness in different atmospheres. The results are in qualitative agreement with the theory. For rods with large surface storage, τ_{rel} increases if the thickness is reduced and becomes very sensitive to the injection level.